Journal of Neuroinflammation

RESEARCH

Open Access

Secoisolariciresinol diglucoside attenuates neuroinflammation and cognitive impairment in female Alzheimer's disease mice via modulating gut microbiota metabolism and GPER/CREB/BDNF pathway

Mengzhen Jia[1†], Fangjie Ning[1†], Junqing Wen[1], Xiaorui Wang[1], Jiao Chen[2], Jun Hu[2], Xuhui Chen[2*] and Zhigang Liu[1,3*]

Abstract

Background Gender is a significant risk factor for late-onset Alzheimer's disease (AD), often attributed to the decline of estrogen. The plant estrogen secoisolariciresinol diglucoside (SDG) has demonstrated anti-inflammatory and neuroprotective effects. However, the protective effects and mechanisms of SDG in female AD remain unclear.

Methods Ten-month-old female APPswe/PSEN1dE9 (APP/PS1) transgenic mice were treated with SDG to assess its potential ameliorative effects on cognitive impairments in a female AD model through a series of behavioral and biochemical experiments. Serum levels of gut microbial metabolites enterodiol (END) and enterolactone (ENL) were quantified using HPLC-MS. Correlation analysis and broad-spectrum antibiotic cocktail (ABx) treatment were employed to demonstrate the involvement of END and ENL in SDG's cognitive improvement effects in female APP/PS1 mice. Additionally, an acute neuroinflammation model was constructed in three-month-old C57BL/6J mice treated with lipopolysaccharide (LPS) and subjected to i.c.v. injection of G15, an inhibitor of G protein-coupled estrogen receptor (GPER), to investigate the mediating role of the estrogen receptor GPER in the cognitive benefits conferred by SDG.

Results SDG administration resulted in significant improvements in spatial, recognition, and working memory in female APP/PS1 mice. Neuroprotective effects were observed, including enhanced expression of CREB/BDNF and PSD-95, reduced β-amyloid (Aβ) deposition, and decreased levels of TNF-α, IL-6, and IL-10. SDG also altered gut microbiota composition, increasing serum levels of END and ENL. Correlation analysis indicated significant associations between END, ENL, cognitive performance, hippocampal Aβ-related protein mRNA expression, and cortical neuroinflammatory cytokine levels. The removal of gut microbiota inhibited END and ENL production and

[†]Mengzhen Jia and Fangjie Ning contributed equally to this work.

*Correspondence:
Xuhui Chen
xuhuichen@pkuszh.com
Zhigang Liu
zhigangliu@nwsuaf.edu.cn

Full list of author information is available at the end of the article

eliminated the neuroprotective effects of SDG. Furthermore, GPER was found to mediate the inhibitory effects of SDG on neuroinflammatory responses.

Conclusion These findings suggest that SDG promotes the production of gut microbial metabolites END and ENL, which inhibit cerebral β-amyloid deposition, activate GPER to enhance CREB/BDNF signaling pathways, and suppress neuroinflammatory responses. Consequently, SDG exerts neuroprotective effects and ameliorates cognitive impairments associated with AD in female mice.

Keywords Secoisolariciresinol diglucoside, Alzheimer's disease, Cognitive impairment, GPER, Gut microbiota, Neuroinflammation

Introduction

With the intensification of the global aging population trend, the prevalence of Alzheimer's disease (AD) is showing a trend of accelerated growth. AD is the most common form of dementia, characterized by the excessive deposition of β-amyloid (Aβ) and the neurofibrillary tangle. Additionally, core features such as neuroinflammation [1] and synaptic dysfunction [2] play crucial roles in the occurrence and development of physiological impairments associated with AD. Over the years, epidemiological studies have indicated that, regardless of age and ethnicity, female patients with AD account for two-thirds of the total patient population [3, 4]. Women in premenopausal, perimenopausal, or postmenopausal stages are more susceptible to developing AD, indicating a correlation between gender factors and the attenuation of estrogen signaling in the pathogenesis of AD [5]. As a neuroactive steroid hormone, estrogen exerts neuroprotective effects by reducing Aβ and glutamate toxicity [6], enhancing synaptic plasticity, maintaining neuronal nutritional components, facilitating transcription factor initiation, reducing brain inflammation [7, 8], and decreasing tau protein hyperphosphorylation [9–11], thereby ameliorating cognitive impairments associated with brain aging [5, 12]. In recent years, estrogen replacement therapy (HRT) has demonstrated significant potential as an intervention approach for AD [13]. However, considering the side effects of HRT, such as an increased risk of stroke and venous thromboembolism [13, 14], phytoestrogens appear to be a promising alternative [15].

Secoisolariciresinol diglucoside (SDG) is the principal component of lignans in flaxseed, belonging to the phytoestrogen family [16]. SDG content is remarkably high in flaxseeds, ranging from 1 to 4% (*w/w*) [17, 18]. The study indicates that SDG alleviates the pathological features of postmenopausal osteoporosis model mice induced by ovariectomy, and its mechanism of action involves phytoestrogenic effects and anti-inflammatory properties [19]. Moreover, SDG exerts protective effects by inhibiting inflammation in various diseases, including peripheral local inflammatory diseases such as osteoarthritis [20], colitis [21, 22], postmenopausal osteoporosis [19], atopic dermatitis [23], as well as systemic and neural inflammation induced by LPS [24, 25]. Additionally, dietary supplementation of SDG effectively alleviates depressive-like behavior in ovariectomized mice exposed to chronic stress. This may be partially attributed to its inhibitory effects on neuroinflammatory responses and its promotion of brain-derived neurotrophic factor (BDNF) expression [26]. SDG has the potential to extend the lifespan of *C. elegans* and protect them from the toxic effects induced by $A\beta_{1-42}$ [27]. However, it remains unclear whether SDG can alleviate cognitive impairments and pathological features associated with AD in females.

Flaxseed lignan SDG is metabolized by bacteria in the colon to the biologically active lignans, enterodiol (END) and enterolactone (ENL) [28, 29]. The structures of END and ENL are analogous to the endogenous estrogen estradiol. This structural similarity elucidates their ability to bind to estrogen receptors and exhibit weak estrogenic effects [16]. The study found that the biological effects of SDG partially depend on the production of endogenous estrogen-like compounds, such as END and ENL, as well as the activation of the GPER [30, 31]. GPER is a 7-transmembrane protein that recognizes and transduces estrogen signals, structurally unrelated to estrogen receptor (ER) α/β [32]. GPER is widely expressed in systemic tissues, with high expression in the central nervous system including the hippocampus, cortex, and hypothalamus [33–37]. In addition, ERα requires GPER to exert neuroprotective effects, while GPER can exert beneficial effects on Parkinson's disease independently of ERα/β [38]. Similarly, activation of GPER significantly enhances recognition memory in female 5XFAD mice [39]. In the brain, microglial cells exhibit high levels of GPER expression, and their activation can downregulate Toll-like receptor 4 expression and reduce the release of inflammatory cytokines [40, 41]. Furthermore, GPER activation is involved in hippocampal-dependent spatial memory [42], synaptic plasticity [43] and the expression of neurotrophic factors. Therefore, here it was hypothesized that SDG may exert neuroprotective effects by activating GPER through its gut microbial metabolites END and ENL, thereby rescuing cognitive impairments associated with AD in females.

Herein, female APPswe/PSEN1dE9 (APP/PS1) mice were treated with SDG to preliminarily investigate the potential of SDG in ameliorating cognitive impairment and neuropathology, including the expression of postsynaptic density protein-95 (PSD-95) and BDNF, Aβ deposition, and neuroinflammation. The regulatory effects of SDG on gut microbiota composition and its metabolites END/ENL were also explored. Subsequently, to investigate the key role of END and ENL in SDG attenuating cognitive impairment in female APP/PS1 mice, broad spectrum antibiotic cocktail (ABx) treatment was performed to remove the gut microbiota and inhibit the production of END and ENL. Finally, the potential involvement mechanisms of GPER in the SDG-mediated amelioration of neuroinflammation associated with AD was examined by using G15, a GPER antagonist, in an LPS-induced neuroinflammation animal model.

Materials and methods

Animals

Ten-month-old female APP/PS1 mice, wild-type (WT) mice and the three-month-old female C57BL/6J mice were procured from the model animal research center of Beijing HFK Biotechnology Co., LTD. DNA samples were extracted from mouse ears and genotyped using polymerase chain reaction (PCR) methodology (DNA extraction kit, centrifugal column method; Beijing Betek Biotechnology Co. LTD, Beijing, China). All mice were housed individually in cages under standard laboratory conditions with a 12/12-h light-dark cycle, at a temperature of 22±2 °C, and a relative humidity of 55±5%. Additionally, the mice utilized in the experiment were bred in-house. The Animal Ethics Committee of Northwest A&F University (authorization number: XN2023-0716) approved the experimental protocol.

Experimental design

Experiment 1 (SDG intervention)

Ten-month-old female APP/PS1 mice and their litter control WT mice were randomly assigned to the following groups: (A) WT+Vehicle group (n=10); (B) WT+SDG group (n=9); (C) APP/PS1+Vehicle group (n=6); (D) APP/PS1+SDG group (n=7). SDG (70 mg/kg) was administered orally once daily at the same time, while the control group received saline [44, 45]. The body weight of mice was measured weekly, along with monitoring of food intake and water consumption. Behavioral tests were conducted after the 8th week. Following anesthesia, serum samples were collected from retro-orbital bleeding. Brains were then extracted to separate the cortex and hippocampus, with collection of other tissues as necessary.

Experiment 2 (ABx treatment)

Ten-month-old female APP/PS1 mice were randomly allocated to the following groups: (A) APP/PS1 group (n=5); (B) APP/PS1+SDG group (n=5); (C) APP/PS1+ABx+SDG group (n=5).

In brief, mice were treated with an ABx containing Penicillin G sodium (1 g/L), metronidazole (1 g/L), neomycin sulfate (1 g/L), streptomycin sulfate (1 g/L), and gentamicin hydrochloride (0.5 g/L). Solutions and bottles were changed twice weekly. Mice received 2 weeks of ABx before the SDG intervention. Microbiota depletion was confirmed by the fecal genome DNA extraction kit (DP328-02) and quantitative real-time PCR (qRT-PCR). qRT-PCR was performed with the universal bacteria-specific primer: (8 F: AGAGTTTGATCCTGGCTCAG; 338R: CTGCTGCCTCCCGTAGGAGT).

SDG (70 mg/kg) was administered orally once daily at the same time, while the control group received saline. Behavioral tests were conducted after the 8th week of intervention.

Experiment 3 (GPER inhibition)

Three-month-old female C57BL/6J mice were randomly allocated to the following groups: (A) Control (CON) group (n=7); (B) LPS group (n=7); (C) LPS+SDG group (n=7); (D) LPS+SDG+G15 group (n=7).

G15 was dissolved in 0.9% saline containing 10% dimethyl sulfoxide (DMSO). 1 μL of this solution at a concentration of 0.5 μg/μL was stereotaxically injected into the lateral ventricle at a rate of 1 μL/min [46–48]. The control group of rats receives stereotactic injection of 1 μL of saline into the lateral ventricle. Following a 2-day recovery period, mice are orally administered SDG (70 mg/kg) or saline for 7 days. In the last 2 days, mice are injected with LPS (0.5 mg/kg; Solarbio) intraperitoneally, according to the previously described method [49]. Injections are spaced 24 h apart, with the CON group receiving injections of saline.

Behavioral experiments

Morris water maze (MWM) test

The water maze experiment consists of two phases: a 3-day spatial acquisition phase followed by a 1-day spatial probe trial. A circular pool, maintained at a temperature of 25 °C, is partitioned into four quadrants. Within one randomly chosen quadrant, a visible platform is positioned 1.5 cm beneath the water surface. Throughout the spatial acquisition phase, mice are introduced sequentially into the pool, facing the wall, from each quadrant. The duration taken by a mouse to successfully ascend onto the platform, termed as escape latency, is monitored using a photobeam tracking system. In instances where a mouse fails to locate the platform within 1 min, it is gently guided to the platform using a probe. Once on

the platform, the mouse remains for 30 s. This sequence is repeated for every quadrant over the span of 3 days. Subsequently, on the spatial probe trial, the platform is removed, and the photobeam tracking system records the number of crossings over the former platform location within 1 min, alongside the time spent and distance traveled in the quadrant where the platform was previously positioned. The movement trajectory of the mice within 1 min is analyzed to evaluate spatial cognitive abilities. Following each trial, mice are dried with a hairdryer and returned to their respective cages.

Barnes maze (BM) test

The BM test was utilized to evaluate the learning and memory capabilities of mice. The BM apparatus comprises a circular platform with 20 equidistant holes along its circumference. One hole contains an escape box serving as a refuge for the experimental animals, while the remaining holes act as visual cues. A bright light source encourages the experimental animals to seek out the escape hole. Adaptation training commenced on day 0, during which mice were given 60 s to familiarize themselves with the escape chamber. Learning trials were conducted from day 1 to 4, each lasting 180 s. Irrespective of whether the mice located the target escape site, they were afforded an additional 60 s of acclimation within the escape chamber. Upon completion of the learning trials, the escape chamber was removed, and the experimental animals were positioned in the center of the elevated platform for a 180 s period of free exploration. The time taken by the experimental animals to locate the correct hole and the frequency of entries into incorrect holes were documented to evaluate spatial reference memory. Moreover, working memory was assessed by recording the number of occasions the animals re-entered incorrect holes. Following each training session, the apparatus underwent cleaning with 75% alcohol, and the correct hole was randomly altered, while maintaining the spatial configuration of the escape chamber constant, to prevent animals from relying on olfactory cues.

Novel object recognition (NOR) test

The NOR test serves as a method to evaluate the short-term non-spatial recognition memory of experimental animals. The experimental setup comprises a box measuring 60 cm × 60 cm × 46 cm and an automated data collection and processing system. The test encompasses three stages: the adaptation stage, the familiarization stage, and the testing stage. During the adaptation stage (day 1), mice are allowed to freely explore the empty apparatus for 5 min on the training day to minimize their apprehension of the new environment. In the familiarization stage on the second day, two identical objects are positioned diagonally across from each other within the apparatus, and mice are positioned in the center of the testing box. Subsequently, the mice are placed equidistant from the objects and permitted to freely explore for 5 min, with the exploration time on each object recorded. During the testing stage on the third day, one of the objects is substituted with a novel object while retaining its original location, and the exploration time spent on the novel and familiar objects is documented. Upon completion of the experiment, the Preference Index (PI) are computed to evaluate the mice's short-term non-spatial recognition memory. It is noteworthy that following each mouse's completion of the test, the objects undergo disinfection with alcohol and are left to evaporate before reintroducing the mice to eliminate any odor cues left by the mice on the objects.

PI = time to recognize new objects / (time to recognize new objects + time to recognize familiar objects).

Y-maze test

The Y-maze serves as a primary tool for evaluating the working memory abilities, specifically short-term memory, of experimental animals. The experimental apparatus comprises three arms, each forming angles of 120°, with dimensions of 35 cm × 5 cm × 15 cm (length × width × height) per arm. At the initiation of the experiment, mice are introduced into the center of the Y-maze apparatus and permitted to freely explore the maze for a duration of 5 min. Real-time software tracks the total number of arm entries by the mice and records the frequency of consecutive entries into the three different arms. Following each trial, the maze undergoes cleaning with alcohol to eliminate odors, and the alternation percentage is computed using a predefined formula.

Spontaneous alternation = actual number of alternations/ possible number of alternations (defined as the total number of arm entries − 2) × 100%.

Thioflavin S staining

Thioflavin S staining was employed for the detection of amyloid-like protein deposits. Upon euthanasia of the mice, brain tissues were isolated, and one-half of the brain was dissected and placed in vials containing 4% (*v/v*) paraformaldehyde (pH 7.4) for 24 h. Subsequently, the specimens were embedded in paraffin and sectioned into 5 μm slices. Sections underwent deparaffinization in xylene, followed by washes in 100%, 90%, 80%, and 70% ethanol for 5 min each, and three washes with PBS (pH 7.4) for 5 min each. Slices were then permeabilized for 15 min, boiled for 20 min, and washed with PBS for 5 min × 3 times. A 0.5% Thioflavin S solution (CAS#1326-12-1; Shanghai Yuanye Biotechnology Co., Ltd.) was applied to the slices for 8 min. Subsequently, the slices underwent sequential rinses with PBS, 50% ethanol, and PBS for 5 min × 3 times. Finally, the sections were mounted

with DAPI for fluorescence imaging. Slice observation and image acquisition were conducted using an inverted fluorescence microscope (DM5000 B, Germany). Image analysis was performed using Image J software to quantify the area ratio of amyloid-like plaques in the region of hippocampus and cortex.

Quantitative real-time PCR (qRT-PCR)

An appropriate amount of tissue was weighed into 2.0 mL grinding tubes, and BIOZOL (from Hangzhou Bioer Technology Co., China) was incorporated to assess mRNA levels within mouse tissues. NanoDropOne (Thermo Fisher Scientific) was used for quantification. The ueIris II qRT-PCR System First-Strand cDNA Synthesis kit (from US Everbright Inc., Suzhou, China) was utilized to reverse transcribe total RNA into cDNA, and the 2× SYBR Green qPCR Master Mix kit (from US Everbright Inc., China) was used for qRT-PCR to measure mRNA levels. Primer sequences employed are delineated in Table S1. Normalizing Ct values to GADPH and computing relative gene expression levels utilizing the $2^{-\Delta\Delta Ct}$ method.

Western blot (WB) analyses

Brain tissue protein extraction was performed using protein extraction reagents. Tissue total protein was subsequently separated via SDS-polyacrylamide gel electrophoresis and transferred onto polyvinylidene difluoride membranes using a wet transfer apparatus. Following transfer, appropriate antibodies were utilized, and immunoreactive bands were visualized using enhanced chemiluminescence reagents. Information regarding antibodies can be found in Table S2. Immunoreactive bands were captured using enhanced chemiluminescence reagents and scanned utilizing the ChemiDoc XRS imaging system (ChemiDoc™ XRS+, Bio-Rad). Quantitative analysis of the protein blot results was performed using Image J analysis software.

Immunofluorescence staining

The tissue sections were subjected to dewaxing and dehydration using xylene and a gradient of ethanol. Subsequently, the slices were incubated overnight at 4 °C with primary antibodies targeting PSD-95, BDNF, β-amyloid (6E10), and IBA-1. Following the incubation period, the slides were washed with PBS and then incubated with a secondary antibody for 2 h. Information regarding antibodies can be found in Table S2. DAPI was utilized for nuclear staining to seal the sections. Immunofluorescence staining images were acquired using an inverted fluorescent microscope (DM5000 B, Germany). The positive regions were quantified using Image J.

Enzyme-linked immunosorbent assay (ELISA)

Cortex samples were processed for the detection of inflammatory cytokines, such as tumor necrosis factor alpha (TNF-α), interleukin-1 beta (IL-1β), interleukin-6 (IL-6), interleukin-10 (IL-10). All procedures were performed according to the instructions provided with the ELISA kit (xl-Em0359, xl-Em0187, xl-Em0196, xl-Em0201, Xinle Biotechnology, Shanghai, China). A standard curve was generated to calculate the content, which was expressed as ng/g protein.

High-performance liquid chromatography-mass spectrometry (HPLC-MS)

Sample preparation and calibration standards: Blood samples were collected in 1.5 mL plastic microcentrifuge tubes, maintained in a 37 °C water bath, and centrifuged at 3000 rpm for 15 min within 30 min of collection. Serum was transferred into 1.5 mL plastic microcentrifuge tubes and stored at -80 °C. Subsequently, 40 μL of mouse serum was added to 5 mL plastic centrifuge tubes. To extract lignans, 3 mL of ether was added to all samples and stirred for 10 min. The samples were then centrifuged at 1000 g for 5 min and placed at -80 °C for 5–10 min to freeze the serum layer. The upper layer was transferred to 2 mL centrifuge tubes and vacuum dried for approximately 20 min using a centrifugal concentrator (RVC2-18 CDplus). The dried samples were reconstituted in 200 μL of water-acetonitrile mixture (9:1), vortexed for 15 s, and then transferred to Whatman Mini-UniPrep syringeless filter vials (PTFE membrane, 0.2 μm pore size, Fisher Scientific Canada, Ottawa, ON) for HPLC-MS analysis. We followed the detection method previously established for END and ENL in mouse serum [50] and entrusted the detection to the Life Science Research Core Services (Northwest A&F University, Yangling, China).

16 S rRNA gene sequencing

Fecal samples were collected prior to mouse sacrifice. Total DNA from feces was extracted using the E.Z.N.A. fecal DNA extraction kit (Omega Bio-Tek, Norcross, GA). The primers utilized for amplifying the v3–v4 region of 16 S rDNA were as follows: 341 F: CCTACGGGNGGCWGCAG; 806R: GGACTACHVGGGTATCTAAT. Sequencing was performed on the HiSeq platform. Reads underwent quality filtering and were assembled into Tags based on their overlapping relationships. Operational taxonomic units (OTUs) were clustered from the assembled Tags using USEARCH (V7.0.1090). Qiime2 (2018.11), in conjunction with the R Package, was employed to generate a Venn diagram, conduct α-diversity analysis, and create a heatmap and histogram of species abundance. Partial least squares discrimination analysis (PLS-DA) data were produced using the mixOmics package in R (V3.2.1). The 16 S rRNA gene

sequencing analysis detected a total of 875 operational taxonomic units (OTUs). We calculated the LOG2 values for the APP/PS1 + Vehicle and APP/PS1 + SDG groups, and performed t-tests to calculate the p-values for the differential OTUs between the two groups. Subsequently, the bioinformatics analysis platform in the Microbiome Online tool was utilized to generate volcano plot data visualization (https://www.bioinformatics.com.cn/). Furthermore, we specifically analyzed the OTUs annotated at the genus level, which amounted to a total of 397 species.

Statistical analysis

The data were expressed as the mean ± SEM. Statistical analyses were conducted using One-way and Two-way ANOVA followed by Tukey's test (GraphPad Prism 8.0 Software, USA) for comparisons among multiple groups. For the analysis of 16 S rRNA sequencing data, nonparametric tests were applied, specifically a Kruskal-Wallis analysis of variance (ANOVA) test, to identify significant differences among the various groups. The bioinformatics analysis platform in Microbiome Online was employed for correlation data analysis (https://www.bioinformatics.com.cn/). $p < 0.05$ was considered statistically significant.

Results

SDG alleviated cognitive impairment in female APP/PS1 mice

Ten-month-old female APP/PS1 mice were subjected to SDG (70 mg/kg b.w.) gavage for 8 weeks (Fig. 1A). During the experiment, genotype and SDG intervention did not

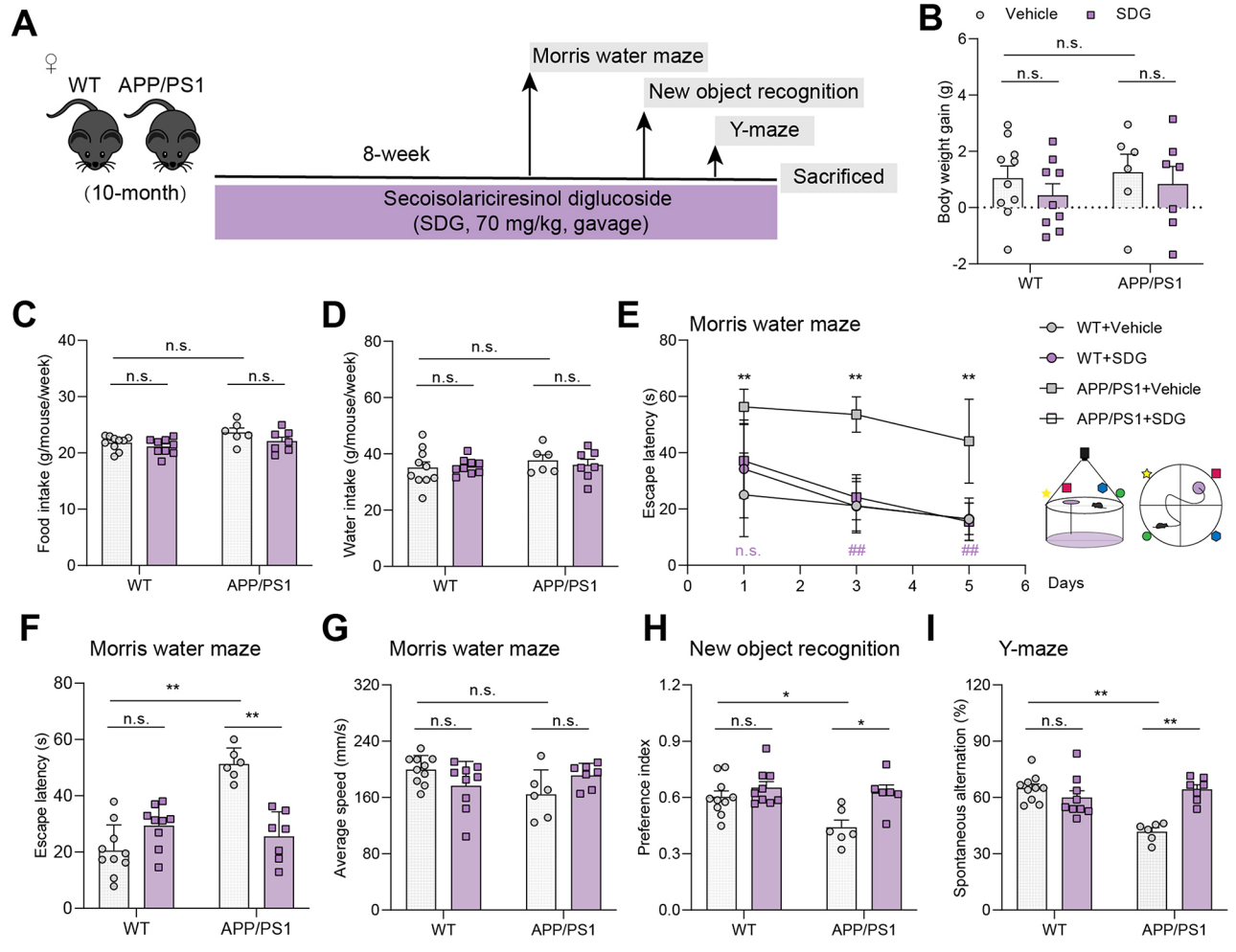

Fig. 1 SDG alleviated cognitive impairment in female APP/PS1 mice. (**A**) Experimental schedule of the SDG intervention in female APP/PS1 mice ($n = 6$–10). (**B**) Body weight gain during the 8-week intervention ($n = 6$–10). (**C**) The average weekly food intake and (**D**) water intake of each mouse ($n = 6$–10). (**E**) Escape latency change during the MWM test training days ($n = 6$–10, $^{*}p < 0.05$, $^{**}p < 0.01$, compared to the WT + Vehicle group, $\#p < 0.05$, $\#\#p < 0.01$, compared to the APP/PS1 + Vehicle group). (**F**) Escape latency and (**G**) average speed on the testing day ($n = 6$–10). (**H**) Preference index in the NOR test ($n = 6$–10). (**I**) Spontaneous alternation (%) in the Y-maze test ($n = 6$–10). Data are presented as mean ± SEM and were analyzed using two-way ANOVA with Tukey's test. $^{*}p < 0.05$, $^{**}p < 0.01$, n.s., no significance

significantly affect the body weight gain, food intake, and water intake of each group of mice (Fig. 1B-D).

To investigate the alleviating effect of SDG on cognitive impairment in female APP/PS1 mice, MWM tests, NOR tests, and Y-maze tests were conducted. During the training period of the MWM test on the 1st, 3rd, and 5th day, compared to the WT + Vehicle group mice, the APP/PS1 + Vehicle group mice showed a significant increase in escape latency (Fig. 1E, $p < 0.01$), indicating significant spatial memory impairment in the APP/PS1 + Vehicle group mice. However, the SDG intervention significantly decreased the escape latency in female APP/PS1 mice but not in the WT mice (Fig. 1E) ($p < 0.01$). On the 6th day, the platform was removed for the probe trial. Similarly, in the probe trail, the APP/PS1 + Vehicle group mice showed a longer escape latency (Fig. 1F) ($p < 0.01$). However, SDG intervention significantly reversed this spatial memory impairment in female APP/PS1 mice (Fig. 1F) ($p < 0.01$). Notably, alleviation of this phenotype upon SDG intervention was not affected by the swimming speed of mice (Fig. 1G). In addition, in the NOR test, the APP/PS1 group mice also showed a lower preference index, indicating their recognition memory were impaired (Fig. 1H) ($p < 0.05$). SDG intervention significantly increased the preference index of female APP/PS1 mice (Fig. 1H) ($p < 0.05$). The result of the Y-maze test used to evaluate spatial working memory showed that compared to the WT + Vehicle group mice, female APP/PS1 mice had significantly reduced spontaneous alternation (Fig. 1I) ($p < 0.01$), while SDG intervention significantly increased spontaneous alternation in female APP/PS1 mice (Fig. 1I) ($p < 0.01$). These results illustrated that the SDG intervention significantly rescued the spatial memory, recognition memory, and the working memory in female APP/PS1 mice.

The common pathological features of AD also include synaptic abnormalities and functional impairments, which occur in the early stages of the disease [51]. To examine whether SDG intervention affected synaptic function in the female APP/PS1 mice, synaptic plasticity-related proteins, including PSD-95 was assessed by immunofluorescence staining. Representative images and quantitative results show that the positive area of PSD-95 protein in the hippocampal dentate gyrus (DG) and cortex of female APP/PS1 mice is significantly lower than that of WT mice (Fig. 2A-C) ($p < 0.01$). However, SDG intervention significantly increased the expression levels of PSD-95 protein in these two regions of female APP/PS1 mice (Fig. 2A-C) ($p < 0.01$).

BDNF plays a crucial role in maintaining synaptic plasticity in learning and memory [52]. In the pathological process of AD, BDNF and CREB are key downstream mediators of Aβ toxicity [53]. And Aβ decreases BDNF primarily by reducing phosphorylated CREB protein [53]. Therefore, to clarify the effect of SDG intervention on CREB-BDNF signaling pathway, the expression levels of BDNF in the hippocampal DG and cortex were analyzed through immunofluorescence staining, and analyzed the expression levels of p-CREB and CREB proteins through WB. The results showed that SDG intervention promoted BDNF expression in female WT and APP/PS1 mice (Fig. 2D-F) ($p < 0.01$). Consistently, the mRNA expression levels of PSD-95 and BDNF in the hippocampus were significantly upregulated by SDG intervention (Fig. 2G-H) ($p < 0.05$). Moreover, SDG intervention significantly activated p-CREB (Fig. 2I & J) ($p < 0.05$). These results indicate that SDG intervention may increase PSD-95 protein expression by activating the CREB-BDNF signaling pathway, thereby alleviating cognitive impairment in female APP/PS1 mice.

SDG reduced Aβ deposition and neuroinflammatory response

Aβ deposition is one of the main pathological features of AD. To investigate the influence of SDG on Aβ deposition in female APP/PS1 mice, the brain sections were stained by Thioflavin S staining and immunofluorescence staining with an anti-6E10 antibody (Fig. 3A and Figure S1A). Compared to the APP/PS1 + Vehicle group mice, the mice treated with SDG showed a remarkable decrease of Aβ deposition in the DG of the hippocampus and the cortex (Fig. 3B-C and Figure S1B-C). Consistently, the mRNA expressions of amyloid precursor protein (APP), Presenilin-1 (PS1), in the hippocampus of female APP/PS1 mice were higher than the WT mice (Fig. 3D-E) ($p < 0.01$), while SDG remarkably downregulated the expression of these genes (Fig. 3D-E) ($p < 0.01$). In addition, SDG significantly downregulated the mRNA expression of β-secretase (BACE1) (Fig. 3F) ($p < 0.05$). Therefore, SDG intervention reduced the accumulation of Aβ in female APP/PS1 mice brain.

Neuroinflammation has demonstrated to be crucial to the pathogenesis of AD, and among the innate immune cells, microglia are the primary players in neuroinflammation [54]. Here, whether SDG can inhibit the neuroinflammatory response in female APP/PS1 mice was further investigated. It has been found that the number of ionized calcium binding adapter molecule 1 (IBA-1) positive cell was significantly increased in the DG of the hippocampus and the cortex in female APP/PS1 mice compared to the WT mice (Fig. 3G-I) ($p < 0.01$). Obviously, compared to the vehicle-treated APP/PS1 mice, SDG significantly reduced the number of IBA-1 positive cells in these two regions (Fig. 3G-I) ($p < 0.01$). Although the levels of pro-inflammatory cytokines such as TNF-α and IL-6 did not show statistically significant differences in the cortex of WT + Vehicle and APP/PS1 + Vehicle groups mice, SDG intervention significantly reduced their expression in the cortex of female APP/PS1 mice

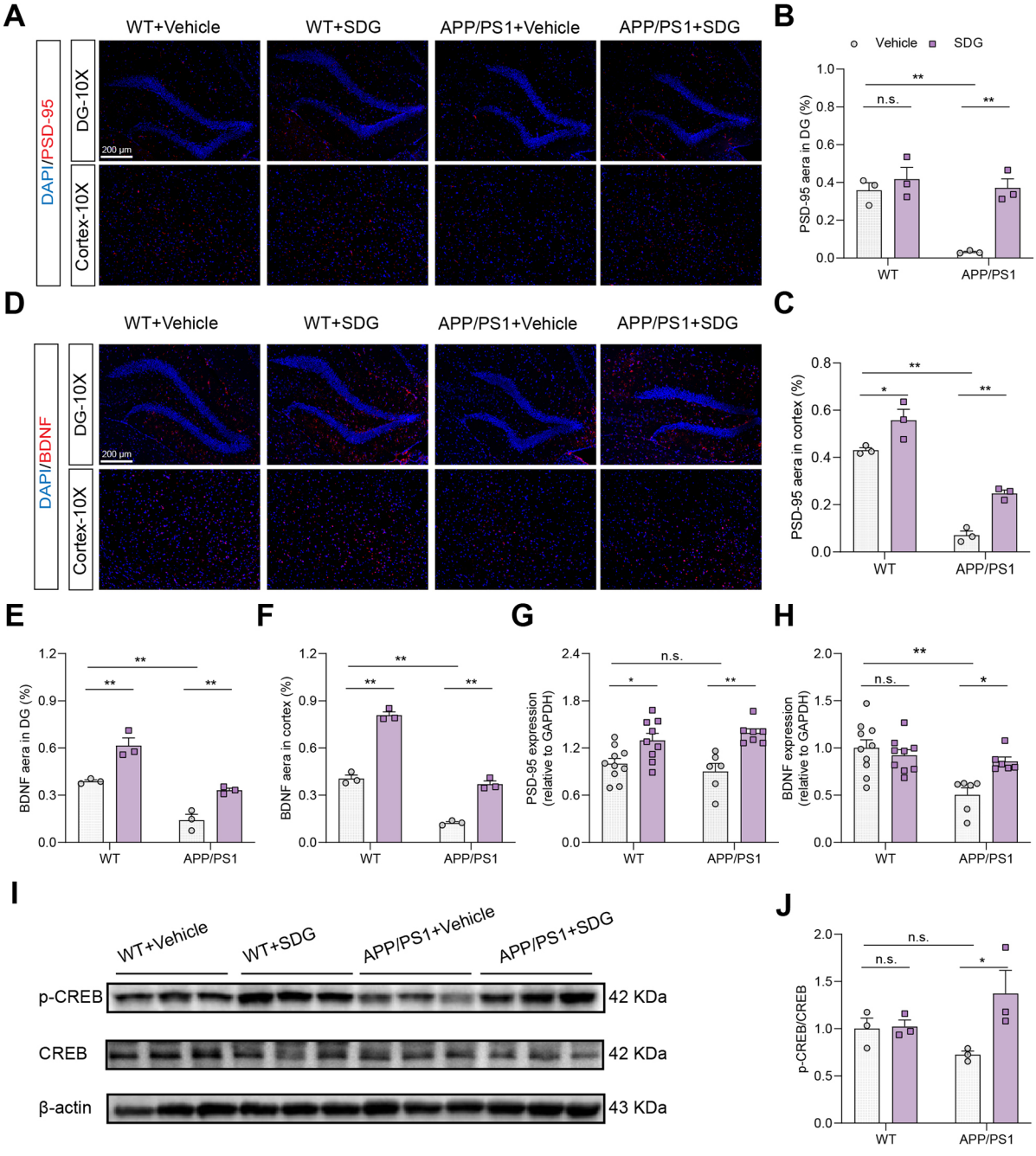

Fig. 2 SDG promoted the expression of synapse-related protein and BDNF. (**A**) Representative images of PSD-95 immunofluorescence staining in the hippocampal DG and cortex.(**B**) and (**C**) Quantification of PSD-95 positive area based on immunofluorescence staining sections by ImageJ software ($n=3$). (**D**) Representative images of BDNF immunofluorescence staining in the hippocampal DG and cortex. (**E**) and (**F**) Quantification of BDNF positive area based on immunofluorescence staining sections by ImageJ software ($n=3$). (**G**) and (**H**) The mRNA expression levels of PSD-95 and BDNF in the hippocampus region ($n=6$–10). (**I**) and (**J**) Protein levels of CREB and p-CREB in the cortex ($n=3$). Data are presented as mean ± SEM and were analyzed using two-way ANOVA with Tukey's test. *$p<0.05$, **$p<0.01$, n.s., no significance

(Fig. 3J-K) ($p<0.05$). In addition, SDG intervention significantly increased the levels of anti-inflammatory cytokine such as IL-10 in the cortex of female APP/PS1 mice (Fig. 3L) ($p<0.05$). Interestingly, compared to WT mice, the levels of IL-10 were significantly correlated in the cortex of female APP/PS1 mice (Fig. 3L) ($p<0.05$). These results indicate that central immune homeostasis is disrupted in female APP/PS1 mice, possibly associated with an imbalance in pro-inflammatory and anti-inflammatory cytokine levels. The SDG intervention contributes to

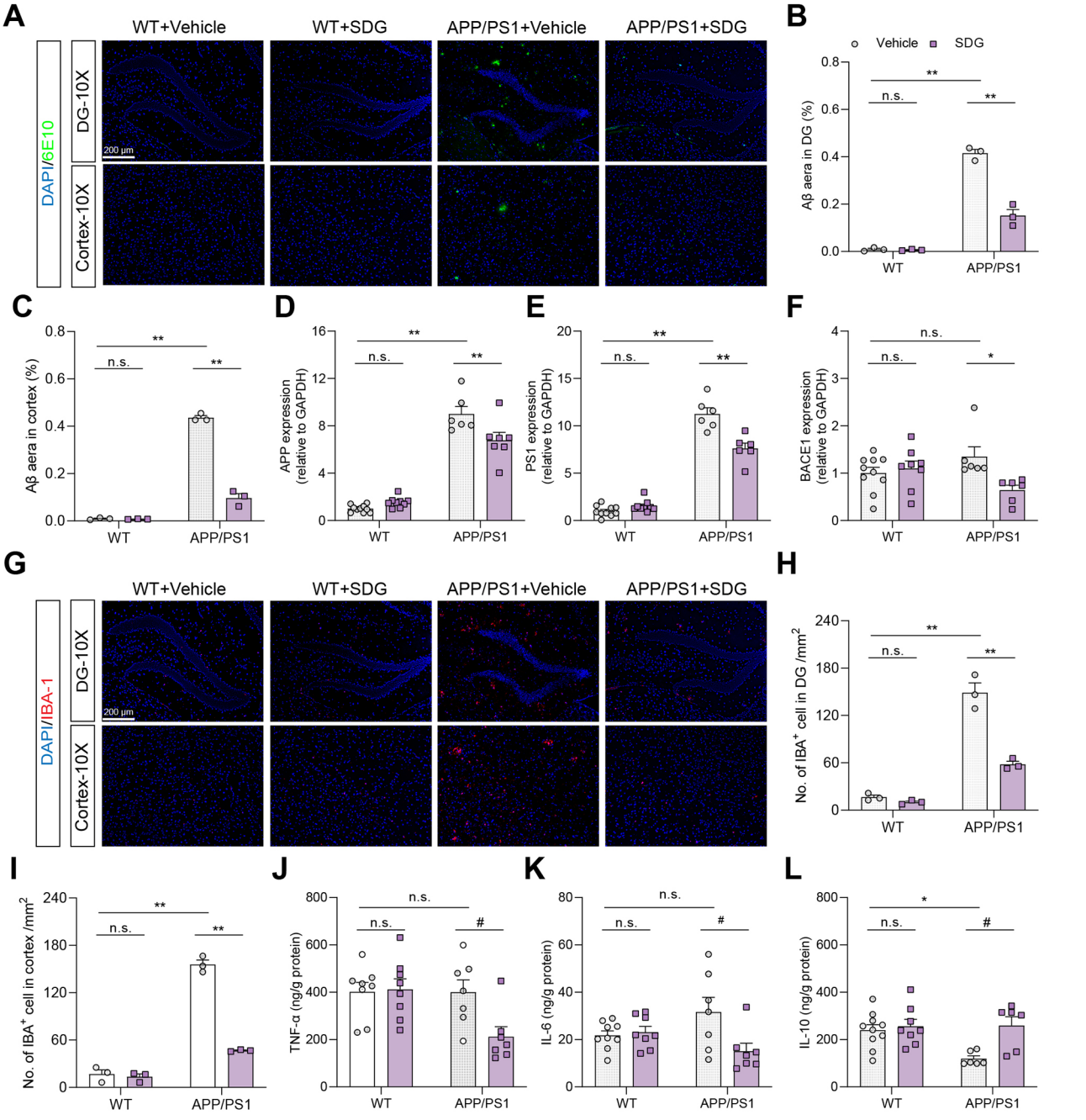

Fig. 3 SDG reduced Aβ deposition and neuroinflammatory response. (**A**) Representative images of Aβ plaques immunofluorescence staining in the hippocampal DG and cortex. (**B**) and (**C**) Quantification of Aβ deposition area based on immunofluorescence staining sections by ImageJ software ($n = 3$). (**D**) – (**F**) The mRNA expression levels of APP, PS1, and BACE1 in the hippocampus region ($n = 6$–10). (**G**) Representative images of IBA-1 immunofluorescence staining in the hippocampal DG and cortex.(**H**) and(**I**) Quantification of the number of IBA-1 positive cells based on immunofluorescence staining sections by ImageJ software ($n = 3$). (**J**) – (**L**) The levels of TNF-α, IL-6, and IL-10 in the cortex ($n = 6$–10). Data are presented as mean ± SEM and were analyzed using two-way ANOVA with Tukey's test. *$p < 0.05$, **$p < 0.01$, n.s., no significance

regulating central immune homeostasis in female APP/PS1 transgenic mice, thereby suppressing neuroinflammatory responses.

SDG reshaped the composition of gut microbiota

SDG reaches the colon, where it is catalyzed by the gut microbiota for metabolism [55]. Therefore, it was speculated that the potential cognitive improvement effect of SDG on AD may be attributed to its influence on the composition of the gut microbiota or its metabolites produced by the gut microbiota. To validate this hypothesis, the gut microbiota structure alteration after SDG treatment was firstly investigated by conducting 16 S rRNA gene sequencing on fecal samples from mice.

The species accumulation curve results indicate that the detected sample size is sufficient to reflect the species composition of the community (Figure S2A). In the four groups of mice, WT + Vehicle, WT + SDG, APP/PS1 + Vehicle, and APP/PS1 + SDG, 796, 801, 754, and 764 OTUs were detected, respectively (Fig. 4A). There were 45 and 37 specific OTUs in the WT + Vehicle group and APP/PS1 + Vehicle group, respectively. Besides, compared to the APP/PS1 + Vehicle group, there were 63 specific OTUs in the APP/PS1 + SDG group (Fig. 4A). The α-diversity analysis including Ace, Chao, coverage, Shannon, Simpson, and Sobs indices indicate that the abundance of gut microbiota in each group of mice is relatively high, with good evenness, and no significant differences are observed among the groups (Figure S2B). Both unweighted and weighted UniFrac analyses of β-diversity indicate significant differences in the gut microbiota community structure between the APP/

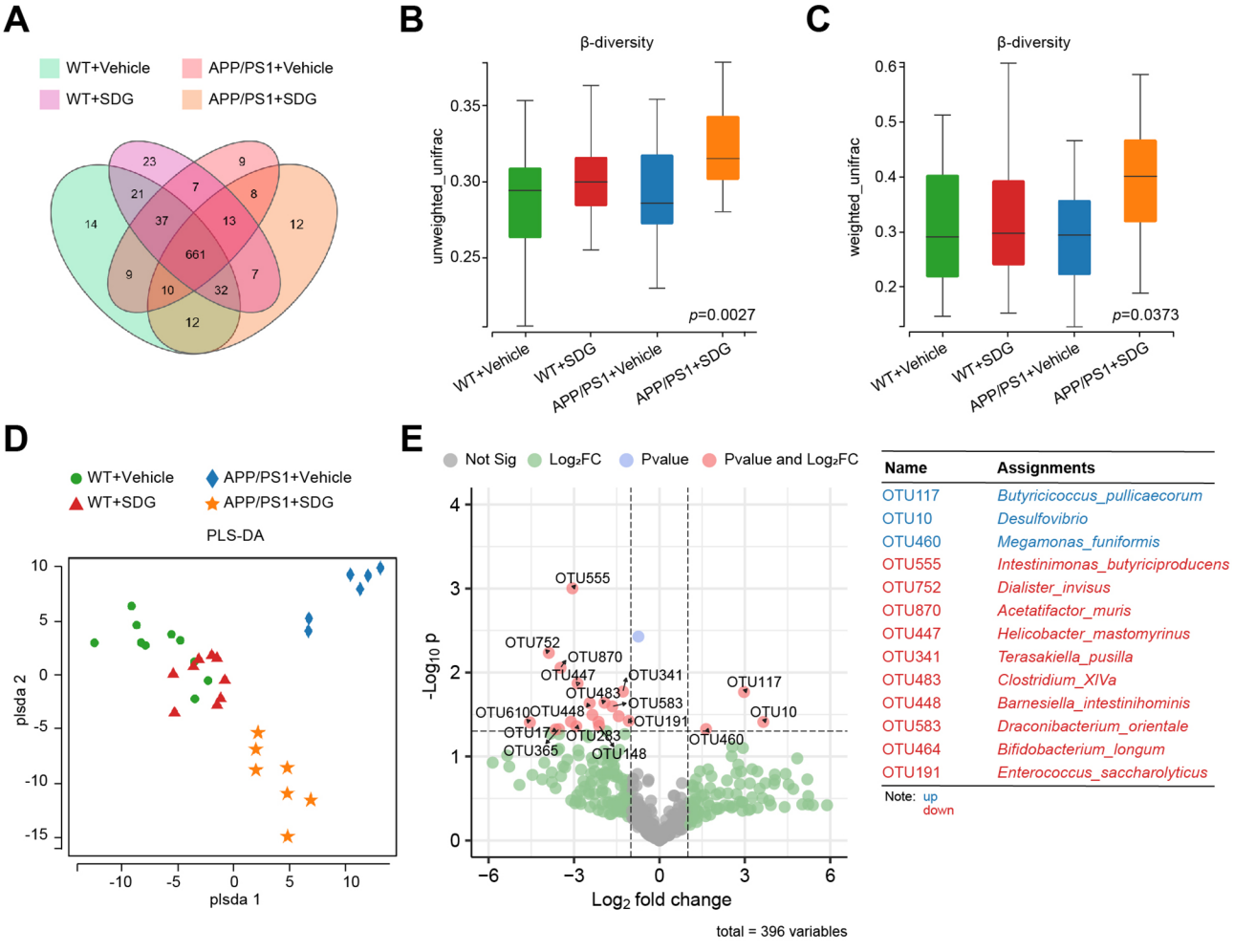

Fig. 4 The effect of SDG on the gut microbiota composition. (**A**) Venn diagrams illustrating the discrepancy of OTUs. (**B**) – (**C**) Beta diversity index box (unweighted unifrac and weighted unifrac). The five lines from bottom to top are minimum, first quartile, median, third quartile, and maximum. (**D**) The result of Partial least squares discrimination analysis (PLS-DA) of each group. (**E**) Volcano plot of differential Relative abundance of OTUs in APP/PS1 + Vehicle and APP/PS1 + SDG group (grey represents not significant; green represents a significant Log2FC value; blue represents a significant p value; and red represents significant Log2FC value and *p* value). On the right side of the volcano plot, the top 3 OTUs (in blue font) with significantly increased and the top 10 OTUs (in red font) with significantly decreased were listed. The default *p*-value threshold is 0.05, and the default FC threshold is 2.0

PS1+Vehicle and APP/PS1+SDG groups (Fig. 4B & C) ($p<0.05$). In addition, the partial least squares discrimination analysis (PLS-DA) plot illustrated a clear and separate clustering of the samples among different groups (Fig. 4D). We calculated the Log2FC values and *p*-values (using a T-test) for the relative abundance of OTUs in the APP/PS1+Vehicle and APP/PS1+SDG groups, and generated the volcano plot in Fig. 4E. And the volcano plot displays 396 OTUs with taxonomic annotations at the species and genus levels. We focused on the OTUs with significant Log2FC values and p-values (highlighted with pink circular markers). Three OTUs (*Butyricicoccus pullicaecorum*, *Desulfovibrio*, and *Megamonas funiformis*) with significantly increased relative abundance in the APP/PS1+SDG group compared to the APP/PS1+Vehicle group are listed (in blue font). Additionally, the top 10 OTUs with significantly decreased relative abundance in the APP/PS1+SDG group are listed as *Intestinimonas butyriciproducens*, *Dialister invisus*, *Acetatifactor muris*, *Helicobacter mastomyrinus*, *Terasakiella pusilla*, *Clostridium XlVa*, *Barnesiella intestinihominis*, *Draconibacterium orientale*, *Bifidobacterium longum*, and *Enterococcus saccharolyticus* (in red font). The comprehensive results indicate that SDG has effects on the composition of the gut microbiota in female APP/PS1 mice.

The cognitive improvement effect of SDG depended on the existence of gut microbiota

In general, whether in humans or other mammals, SDG undergoes a series of biotransformation processes through colonic microbiota, ultimately metabolizing into END and ENL [50]. To assess the metabolic levels of SDG by the gut microbiota, the levels of END and ENL in serum were detected by using HPLC-MS. The results showed that SDG intervention increased the content of END and ENL in the serum of female WT and APP/PS1 mice (Fig. 5A & B) ($p<0.01$). To further analyze the relationship between these two metabolites and SDG in enhancing cognitive function, inhibiting Aβ deposition, and neuroinflammatory responses, the correlation analysis on the relevant data from the APP/PS1+Vehicle and APP/PS1+SDG groups was conducted (Fig. 5C). The correlation analysis results indicate that the levels of END and ENL in serum are significantly negatively correlated with the escape latency in the MWM test (Fig. 5C) ($p<0.05$). Besides, END and ENL are significantly positively correlated with the preference index in the NOR test, spontaneous alternation in the Y-maze (Fig. 5C) ($p<0.05$).

To demonstrate the crucial role of gut microbiota and its metabolism in mediating SDG intervention to attenuate AD related cognitive deficits, it sought to investigate whether the beneficial effects of SDG intervention observed after removing gut microbiota in female APP/

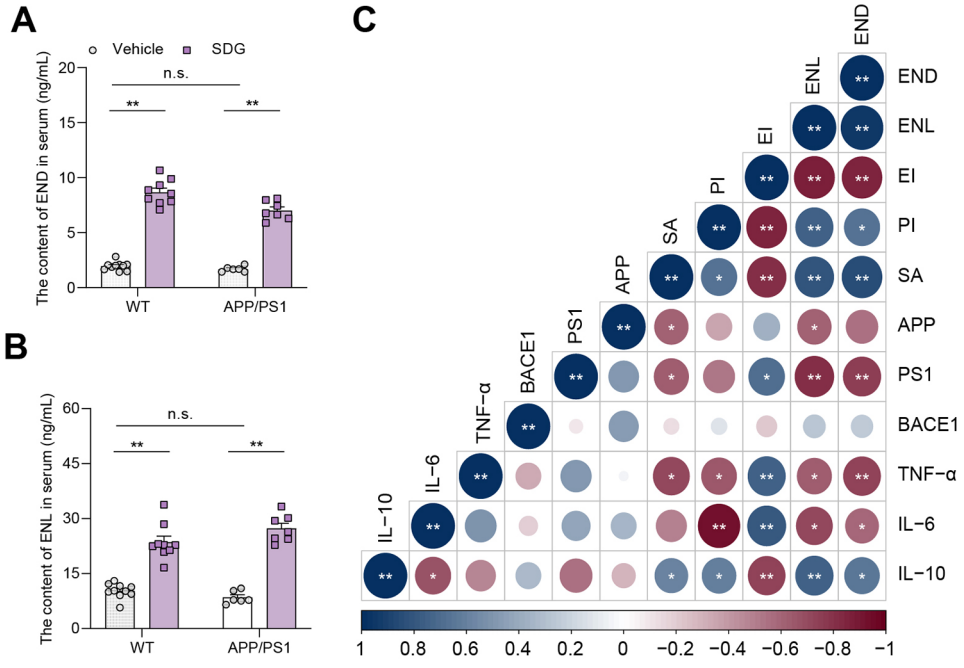

Fig. 5 The gut microbiota-dependent SDG metabolism. (**A**) and (**B**) The levels of END and ENL in the serum. (**C**) Correlation Analysis between the levels of END and ENL in the serum and other biochemical index. In the matrix, the size and color of the circles indicate the degree of correlation (blue represents a positive correlation, and red represents a negative correlation). The calculation method for correlation coefficient is Pearson. *$p<0.05$, **$p<0.01$, and non-significance is not indicated

PS1 mice would be affected (Fig. 6A). 2-week of ABx treatment can effectively remove the gut microbiota of mice and significantly inhibit the in vivo conversion of SDG to END and ENL [56, 57]. After a 2-week treatment of ABx, the copy numbers of 16 S rDNA of the microbiota in the feces of mice in the APP/PS1+ABx+SDG group were significantly lower compared to the other two ABx untreated groups (Fig. 6B) ($p<0.01$). During the experiment, it did not observe any statistically significant changes in body weight gain, food intake, or water intake (Fig. 6C-E). However, the cognitive improvement effect of SDG on AD-related cognition, as observed in the BM test, NOR test, and Y-maze test, was counteracted upon removal of the microbiota (Fig. 6F-J) ($p<0.05$). Furthermore, following SDG intervention, the content of END and ENL in mouse serum significantly decreased with the removal of the microbiota (Fig. 6K-L) ($p<0.01$).

Studies indicate that CREB is downstream of G protein-coupled estrogen receptor 1 (GPER), which serves as the receptor for END and ENL [31, 36]. To elucidate the mediating roles of gut microbiota, END and ENL in the activation of the CREB-BDNF signaling pathway and the increase in PSD-95 protein expression by SDG, the expression of relevant proteins was evaluated through immunofluorescence staining and WB analysis. ABx treatment abolished the promoting effect of SDG on PSD-95 protein expression (Fig. 7A-C) ($p<0.05$) and the activation of the CREB-BDNF signaling pathway (Fig. 7D-H) ($p<0.05$). In conclusion, these findings suggest that the neuroprotective effect of SDG on female APP/PS1 mice relies on an intact gut microbiota. Overall, these results showed that the improvement effect of SDG intervention on AD related cognitive impairment depends on the gut microbiota and may be related to its metabolites END and ENL.

The inhibitory effect of SDG on Aβ deposition and neuroinflammation depended on gut microbiota existence

The correlation analysis results also indicate that the levels of END and ENL in serum are significantly negatively correlated with the PS1 mRNA expression levels (Fig. 5C) ($p<0.05$). Furthermore, ENL, but not END, is significantly negatively correlated with APP mRNA expression levels (Fig. 5C) ($p<0.05$). Consistent with this, the reduction of Aβ deposition in the hippocampal DG and cortex of female APP/PS1 mice by SDG was eliminated by ABx treatment (Fig. 8A-C) ($p<0.05$).

The correlation analysis results also indicate that the levels of END and ENL in serum are significantly negatively correlated with the cortical pro-inflammatory cytokines TNF-α and IL-6 levels (Fig. 5C) ($p<0.05$). Besides, END and ENL are significantly positively correlated with the cortical anti-inflammatory cytokine IL-10 level (Fig. 5C) ($p<0.05$). Interestingly, it was observed in female APP/PS1 mice that the escape latency is significantly negatively correlated with cortical TNF-α and IL-6 levels, and positively correlated with IL-10 levels. In contrast, the preference index and spontaneous alternation show an opposite correlation with these inflammatory-related cytokines. Similarly, compared to the APP/PS1+SDG group mice, the APP/PS1+ABx+SDG group mice showed a significant increase in the number of IBA-1 positive cells in the hippocampal DG and cortex (Fig. 8D-F) ($p<0.05$). ABx treatment also disrupted the rebalancing between pro-inflammatory and anti-inflammatory cytokines in the cortex of female APP/PS1 mice established by SDG intervention (Fig. 8G-J) ($p<0.05$).

These results indicate that the inhibitory effect of SDG on Aβ deposition and neuroinflammation in female APP/PS1 mice cannot be separated from the gut microbiota and two metabolites, namely END and ENL.

The activation of GPER was involved in the preventive effect of SDG on LPS-induced neuroinflammation

To further demonstrate the mediating mechanism of GPER in the neuroprotective effect of SDG, G15, an inhibitor of GPER, was injected into the bilateral lateral ventricles of C57BL/6 mice through i.c.v. injection. A 4-day intervention based on SDG was implemented, followed by 3-day of intraperitoneal LPS injection treatment (Fig. 9A). LPS treatment resulted in a significant increase in the mRNA expression levels of hippocampal inflammatory cytokines TNF-α, IL-6, and IL-1β (Fig. 9B-D) ($p<0.05$). However, compared to the control group, there was no significant decrease in hippocampal IL-10 mRNA expression induced by LPS (Fig. 9E). SDG intervention effectively downregulated the mRNA expression of TNF-α, IL-6, and IL-1β, while upregulating the mRNA expression of IL-10 (Fig. 9B-E) ($p<0.05$). Similarly, the inhibitory effect of SDG on neuroinflammation is dependent on the activation of GPER (Fig. 9B-E) ($p<0.05$).

To verify the hypothesis that SDG increases the expression of PSD-95 and BDNF through END and ENL, thereby exerting neuroprotective effects and improving cognitive impairment associated with AD, the mRNA expression levels of PSD-95 and BDNF were assessed. The results indicate that treatment with G15 significantly inhibited the promoting effect of SDG on the cortical mRNA expression of PSD-95 and BDNF in mice with LPS-induced neuroinflammation (Fig. 9F & G) ($p<0.05$).

Overall, these results suggest that GPER plays an indispensable mediating role in the suppression of neuroinflammatory response, and neuroprotective effects exerted by SDG in mice with neuroinflammation models.

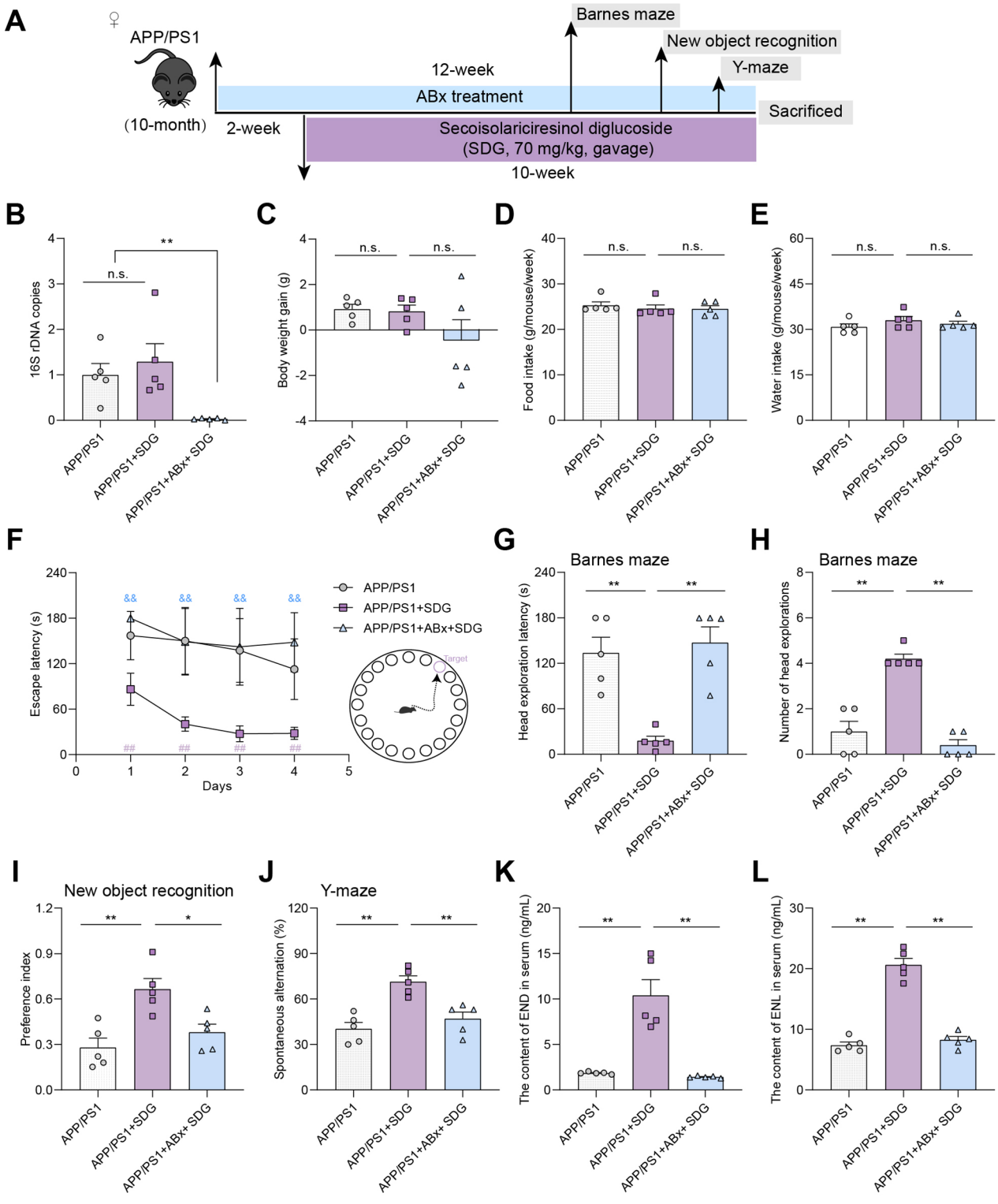

Fig. 6 The cognitive improvement effect of SDG depended on the existence of gut microbiota. (**A**) Experimental schedule of the SDG intervention after the ABx treatment in female APP/PS1 mice ($n=5$). (**B**) The 16 S rDNA copies in the feces ($n=5$). (**C**) Body weight gain during the 8-week intervention ($n=5$). (**D**) The average weekly food intake and (**E**) water intake of each mouse ($n=5$). (**F**) Escape latency change during the BM test training days ($n=5$, #$p<0.05$, ##$p<0.01$, compared to the APP/PS1 group, &$p<0.05$, &&$p<0.01$, compared to the APP/PS1 + SDG group). (**G**) Head exploration latency and (**H**) Number of head explorations on the testing day ($n=5$). (**I**) Preference index in the Novel object recognition test ($n=5$). (**J**) Spontaneous alternation (%) in the Y-maze test ($n=5$). (**K**) and (**L**) The levels of END and ENL in the serum. Data are presented as mean ± SEM and were analyzed using one-way ANOVA with Tukey's test. *$p<0.05$, **$p<0.01$, n.s., no significance

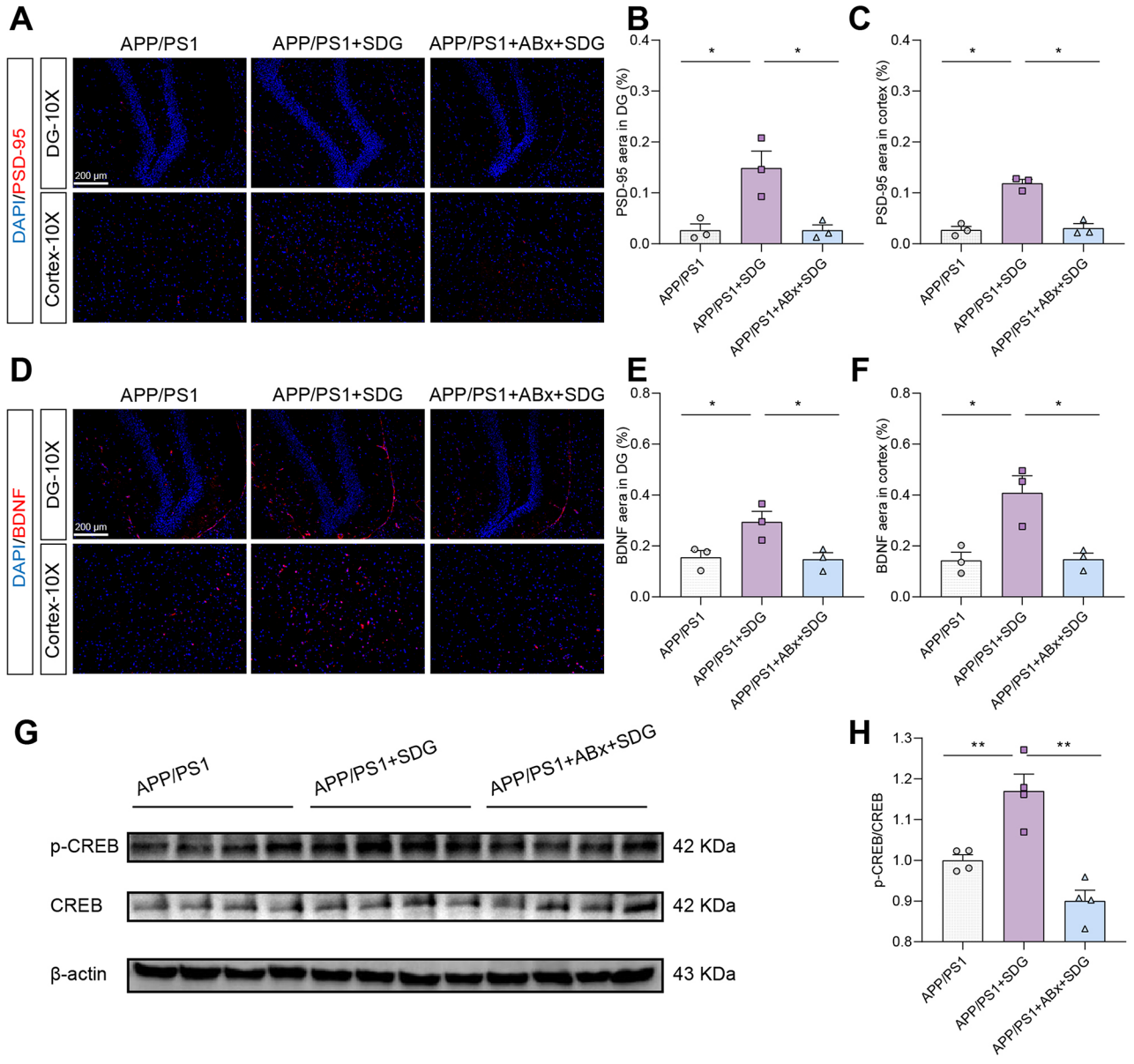

Fig. 7 The promoting effect of SDG on PSD-95 and BDNF expression depended on gut microbiota existence. (**A**) Representative images of PSD-95 immunofluorescence staining in the hippocampal DG and cortex. (**B**) and (**C**) Quantification of PSD-95 positive area based on immunofluorescence staining sections by ImageJ software ($n=3$). (**D**) Representative images of BDNF immunofluorescence staining in the hippocampal DG and cortex. (**E**) and (**F**) Quantification of BDNF positive area based on immunofluorescence staining sections by ImageJ software ($n=3$). G) and H) Protein levels of CREB and p-CREB in the cortex ($n=4$). Data are presented as mean ± SEM and were analyzed using one-way ANOVA with Tukey's test. *$p<0.05$, **$p<0.01$, n.s., no significance

Discussion

In this study, it was found that oral administration of SDG (70 mg/kg) to female APP/PS1 mice increased the expression of BDNF and PSD-95, reduced Aβ deposition in the hippocampal DG and cortex, and suppressed central nervous system inflammation exerting central nervous system protective effects, thereby rescuing cognitive impairments associated with AD in females. Additionally, SDG influenced the composition of gut microbiota and promoted the production of END and ENL. Correlation analysis revealed significant associations between serum levels of END and ENL and cognitive behavioral indices, Aβ expression, neuroinflammation, and other biochemical markers. Furthermore, the neuroprotective effects of SDG were abolished by the inhibition of the production of END/ENL and the GPER activation. These results collectively suggested that the preventive effects of SDG on cognitive impairments and neuroinflammation in female APP/PS1 mice depended on the existence of gut microbiota and microbial metabolites END and ENL, which

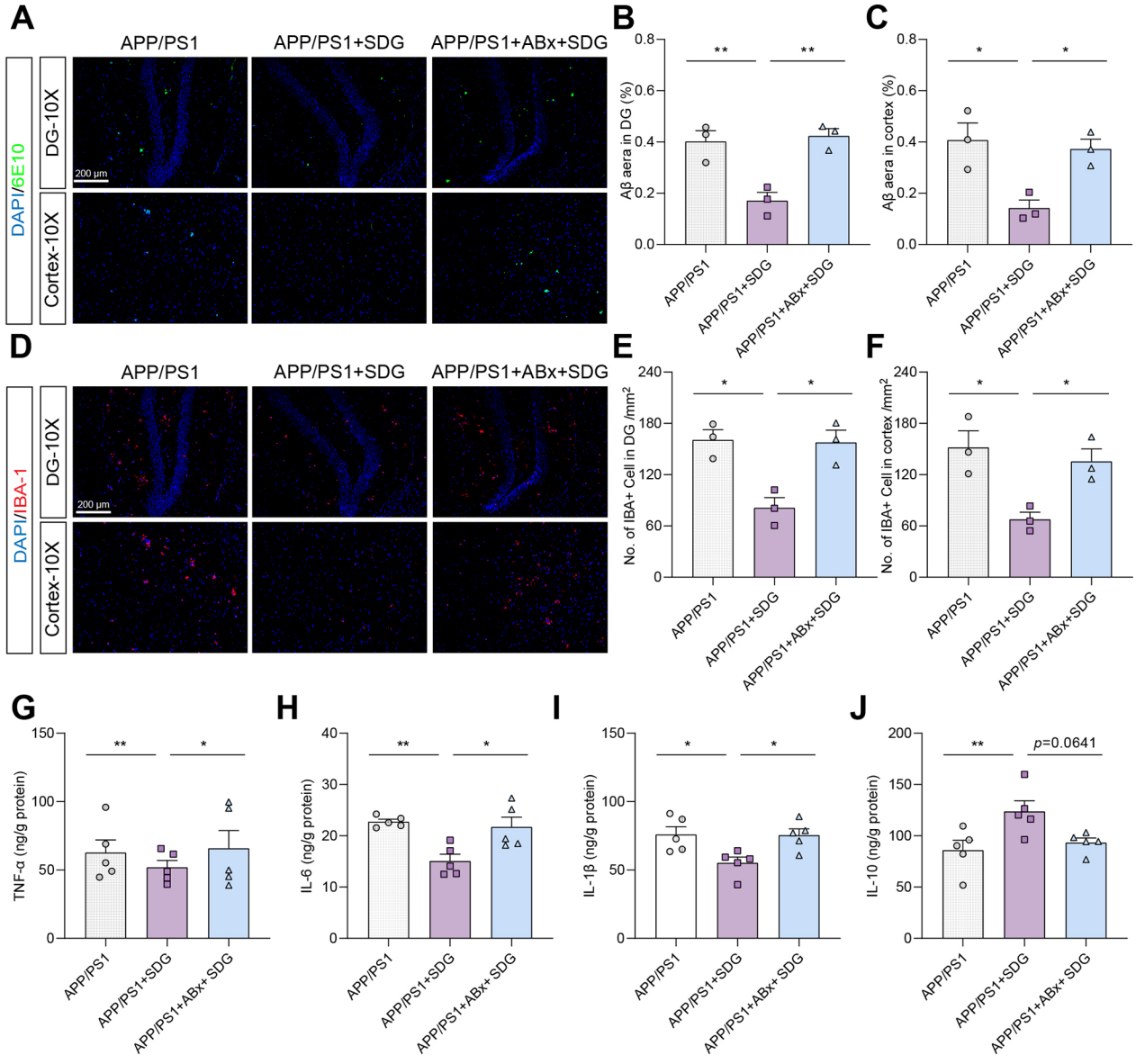

Fig. 8 The inhibitory effect of SDG on Aβ deposition and neuroinflammation depended on gut microbiota existence. (**A**) Representative images of Aβ plaques immunofluorescence staining in the hippocampal DG and cortex. (**B**) and (**C**) Quantification of Aβ deposition area based on immunofluorescence staining sections by ImageJ software ($n = 3$). (**D**) Representative images of IBA-1 immunofluorescence staining in the hippocampal DG and cortex. (**E**) and (**F**) Quantification of the number of IBA-1 positive cells based on immunofluorescence staining sections by ImageJ software ($n = 3$). (**G**) – (**J**) The levels of TNF-α, IL-6, IL-1β, and IL-10 in the cortex ($n = 5$). Data are presented as mean ± SEM and were analyzed using one-way ANOVA with Tukey's test. $^{*}p < 0.05$, $^{**}p < 0.01$, n.s., no significance

consequently activating GPER and down-stream CREB/BDNF pathway.

Numbers of human studies suggest that dietary supplementation with foods rich in SDG may be associated with better cognitive abilities. A study incorporating 394 postmenopausal Dutch women (mean age: 66.3 years) from the PROSPECT study revealed that an increased intake of dietary lignans was associated with better performance on the MMSE [OR and (95% CI): 1.49 (0.94–2.38)] [58]. Another cross-sectional study involving 301 Dutch women aged 60–75 years demonstrated that a high intake of lignans was associated with better performance in processing speed, executive function, and cognitive abilities [59]. Similarly, an observational study on elderly individuals (aged 50 years and above) in Southern Italy found a negative correlation between all individual compounds (excluding SDG) and cognitive impairment [60]. The association between dietary plant estrogens and cognition is multifactorial and may depend on factors such as the cognitive domain assessed and ethnic groups

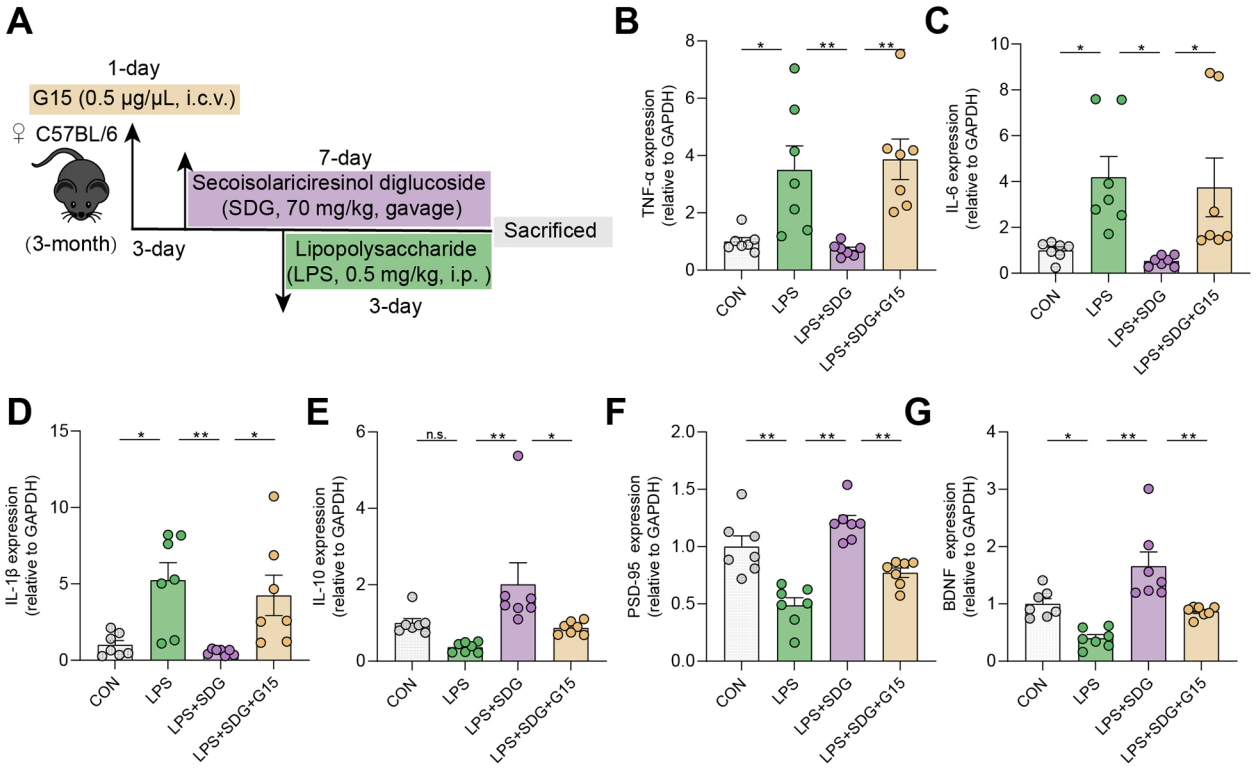

Fig. 9 The activation of GPER was involved in the preventive effect of SDG on LPS-induced neuroinflammation. (**A**) Experimental schedule of the of SDG intervention on LPS induced neuroinflammation mouse model after G15 treatment ($n = 7$). (**B**-**E**) The mRNA expression levels of TNF-α, IL-6, IL-1β, and IL-10 in the hippocampus ($n = 7$). (**F**) and (**G**) The mRNA expression levels of PSD-95 and BDNF in the hippocampus ($n = 7$). Data are presented as mean ± SEM and were analyzed using one-way ANOVA with Tukey's test. *$p < 0.05$, **$p < 0.01$, n.s., no significance

[61]. Although our study has shown that SDG can alleviate cognitive impairment in female AD mice, further exploration is needed in clinical intervention trials targeting female AD patients (Fig. 1E-I).

Research has found that SDG remains stable during the transport process through the upper gastrointestinal tract [55]. Therefore, ingested SDG reaches the distal intestine, where various gut microbes catalyze its metabolism to END and ENL. Culturing flaxseed with human fecal bacteria in vitro can generate END and ENL, while sterile fecal cultures do not produce these metabolites [62]. Moreover, ABx treatment reduces the production of END and ENL in the colon, indicating that the gut microbiota can metabolize plant lignans into gut lignans [62]. A pharmacokinetic study of oral SDG in rats revealed that SDG was undetectable in serum within 48 h [50]. END and ENL reached peak concentrations in serum at 11 and 12 h after oral administration of SDG [50]. Consistent with these results, in the current study, following oral gavage of SDG, there was a significant increase in the levels of END and ENL in the serum of female APP/PS1 mice (Fig. 5A & B). Correlation analysis results indicated a significant correlation between the levels of END and ENL in the serum and cognitive behavioral indices in mice (Fig. 5C). Furthermore, when using ABx treatment to deplete the mouse microbiota to inhibit the production of END and ENL, the beneficial effects of SDG on cognitive improvement in female APP/PS1 mice were abolished (Fig. 6F-L). Our study, for the first time, investigated the effect of SDG on cognitive function in an animal model and found that the alleviative effect in AD-related cognitive dysfunction by SDG is dependent on the gut microbial metabolites END and ENL. In addition, SDG also influenced the β-diversity and the composition of the gut microbiota (Fig. 4A-E). However, the specific role of SDG in shaping the gut microbiota and its effect on the metabolism of SDG to END and ENL remains unclear. Future studies should further investigate the specific mechanisms of microbial transformation of SDG in vivo. In addition, APP/PS1 mice also suffer from gut pathological damage, including impaired gut morphology and barrier function, as well as inflammatory response [63]. Research has shown that SDG has a significant inhibitory effect on high-fat diet induced gut inflammation or Dextran sulfate sodium salt induced colitis [21, 22]. Therefore, it remains to be explored whether SDG can affect gut pathological damage and related mechanisms in AD model mice.

END and ENL share structural similarities with estradiol, one of the most prevalent and potent estrogens [57].

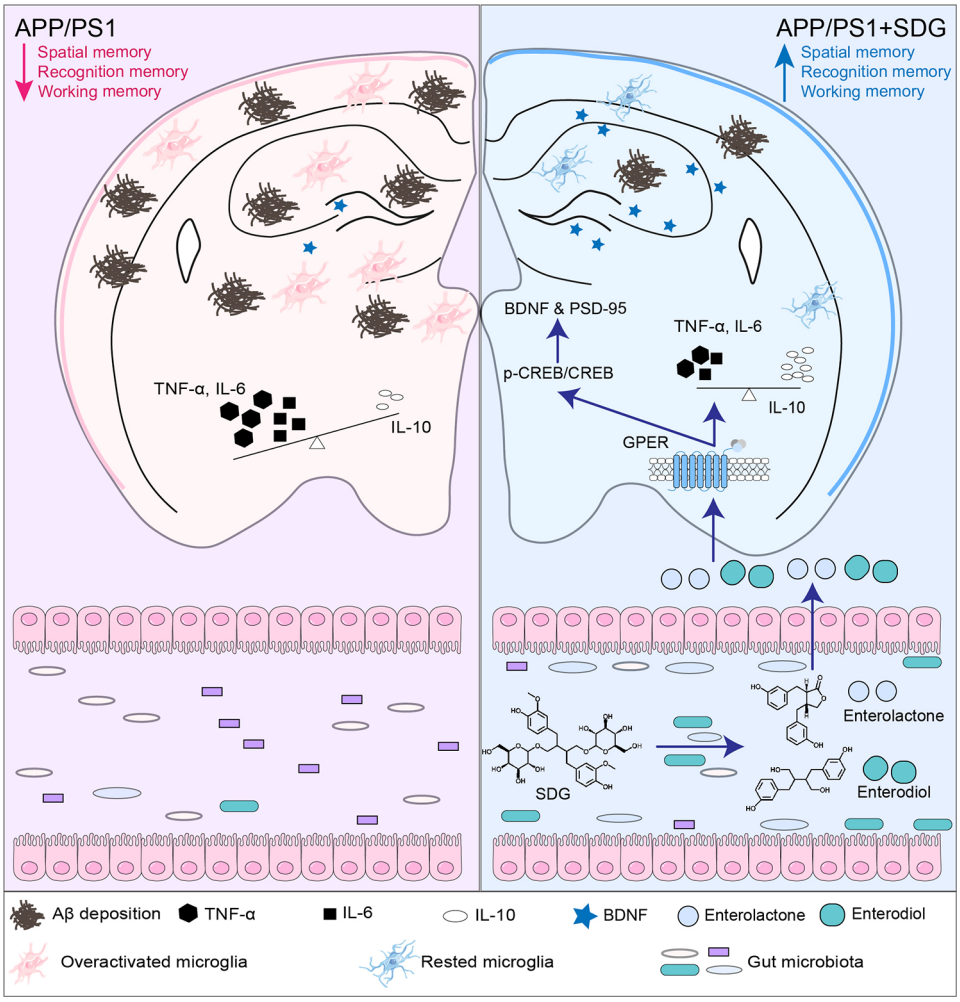

Fig. 10 SDG attenuated cognitive impairment in female APP/PS1 mice SDG is metabolized by gut microbiota to produce END and ENL, which in turn enhance the expression levels of PSD-95 and BDNF, and inhibit neuroinflammatory responses through GPER receptors, and reduce Aβ deposition to enhance the cognitive ability, such as spatial memory, recognition memory, and working memory in the female APP/PS1 mice

GPER, a membrane estrogen receptor [64], is expressed in almost all regions of the brain [37], particularly significantly in the forebrain areas such as the hippocampus and frontal cortex [65]. Additionally, GPER-deficient rats exhibit increased anxiety-like behavior and learning and memory impairments [66]. Therefore, GPER may be involved in memory formation or consolidation. In addition, activation of GPER can inhibit neuroinflammatory responses [67–70], enhance synaptic transmission and plasticity in the hippocampal CA3-CA1 synapse [43, 71], and increase neuronal survival [72]. Furthermore, consistent with our findings, G1, a GPER agonist, effectively alleviated recognition memory impairment in female 5xFAD mice through GPER activation, but not in male mice [39]. Study has found that ENL and END. can effectively activate GPER [30, 31]. Similarly, the activation of GPER depends on the presence of END and ENL (Figs. 2 and 7). However, the neuroprotective effects of GPER may exhibit sexual dimorphism, although no gender-specific differences were observed in GPER expression in 5xFAD mice [39]. Future research on GPER should take gender differences into consideration.

Although the pathogenesis of AD is not completely understood, Aβ deposition remains a major pathological feature of AD. It was found that SDG significantly reduces Aβ deposition in the hippocampal DG region and cortex (Fig. 3A-C, Supplementary Fig. 1). This may be due to the downregulation of mRNA expression of key proteins involved in Aβ production process, including APP, PS1, and BACE1 by SDG (Fig. 3D-F). Correlation analysis results indicated a significant negative correlation between serum END levels and hippocampal PS1 mRNA expression, but no significant correlation with APP and BACE1 mRNA expression (Fig. 5C). On the other hand, ENL showed a significant negative correlation with APP and PS1 mRNA expression, but no significant correlation with BACE1 mRNA expression (Fig. 5C). When the production of END and ENL was inhibited, the

inhibitory effect of SDG on Aβ deposition was also abolished (Fig. 8A-C). Previous study has shown that GPER may be involved in the effects of SDG on Aβ production and deposition [31]. In summary, the preventive effect of SDG on Aβ deposition depends on the activation of GPER by END/ENL.

Dietary supplementation of flaxseed, rather than flaxseed oil, can partially attenuate systemic and neuroinflammation induced by LPS [24]. The absence of SDG in flaxseed oil may be a reason for the differential effects observed between the two interventions [57]. Our research results also indicate that SDG intervention significantly inhibited the neuroinflammatory response in female APP/PS1 mice (Fig. 3G-L). Furthermore, the inhibitory effect of SDG on neuroinflammatory response depends on the production of END and ENL (Fig. 8D-J). Additionally, in an LPS-induced neuroinflammation model in mice, it was observed that SDG downregulates the mRNA expression of TNF-α, IL-6, and IL-1β in the hippocampus, and increases the mRNA expression of IL-10 (Fig. 9B-E). When GPER activation was inhibited by inhibitor G15, the effect of SDG on the expression of hippocampal inflammation-related cytokines mRNA was abolished (Fig. 9B-E). Consistent with our findings, in 1-methyl-4-phenyl-1,2,3,6-tetrahydropyridine-induced animal model of parkinsonism and an in vitro model in BV2 microglial cells, the anti-inflammatory effect including reduced activation of microglia and the abatement of proinflammatory cytokines of G1 was abolished by G15 [68]. These results suggest that SDG may exert neuroinflammatory inhibitory effects by activating GPER through the production of END and ENL, thereby participating in the pathogenesis of AD.

In conclusion, our results provide a solid theoretical basis for the improvement of AD-related cognitive ability by SDG intervention, and the potential mediating mechanisms involving END, ENL, and GPER activation were revealed through ABx treatment removal and intracerebral injection of GPER inhibitor.

Conclusion

In summary, our results indicate that SDG intervention influences the composition of gut microbiota, increases the production of END and ENL, and then inhibits neuroinflammatory response, enhances BDNF and PSD-95 protein expression, and reduces Aβ deposition through GPER receptor activation, thereby rescuing cognitive dysfunction related to the female AD (Fig. 10). Importantly, SDG shows significant potential in delaying the pathological progression of AD in females, providing essential theoretical basis for SDG-related interventions and targeting GPER receptor modulation in the development of AD. Additionally, to avoid wastage of resources, fully exploiting the use of flaxseed meal to extract SDG holds practical and economic value.

Abbreviations

AD	Alzheimer's disease
Aβ	β-amyloid
HRT	Estrogen replacement therapy
SDG	Secoisolariciresinol diglucoside
END	Enterodiol
ENL	Enterolactone
LPS	Lipopolysaccharide
GPER	G protein-coupled estrogen receptor
ER	Rstrogen receptor
BDNF	Brain-derived neurotrophic factor
ABx	Broad spectrum antibiotic cocktail
MWM	Morris water maze
BM	Barnes maze
NOR	New object recognition
qRT-PCR	Quantitative real-time PCR
WB	Western blot
ELISA	Enzyme-linked immunosorbent assay
HPLC-MS	High-performance liquid chromatography–mass spectrometry
DG	Dentate gyrus
APP	Amyloid precursor protein
PS1	Presenilin-1
BACE1	Beta-secretase
IBA-1	Ionized calcium binding adapter molecule 1
TNF-α	Tumor necrosis factor alpha
IL-6	Interleukin-6
IL-1β	Interleukin 1 beta
IL-10	Interleukin-10
PSD-95	Postsynaptic density protein-95

Supplementary Information

The online version contains supplementary material available at https://doi.org/10.1186/s12974-024-03195-4.

Supplementary Material 1: SDG reduces Aβ pathology (Figure S1)； SDG reshapes the composition and structure of gut microbiota (Figure S2)

Supplementary Material 2： Primer sequences used for qRT-PCR (Table S1)

Supplementary Material 3： List of antibodies for immunofluorescence staining and WB (Table S2)

Supplementary Material 4： Original data

Acknowledgements

The authors thanks Yao Liu (Life Science Research Core Services, Northwest A & F University, Yangling, China) for her assistance and detection with HPLC-MS experiments. The author also thanks Dr. Tai An (COFCO Nutrition and Health Research Institute) for providing valuable editing suggestions for the article.

Author contributions

M.J. and F.N. performed the experiments; F.N. analyzed the data; J.W. and X.W. helped with animal experiments. M.J., F.N., X.C., and Z.L. wrote the manuscript; Z.L., M.J. J.H. J.C. and X.C designed the experiments; Z.L. and X.C. gave final content approval. All authors read and approved the final manuscript.

Funding

This work was supported by the Sci-Tech Innovation 2030 Brain Science and Brain-Like Intelligence Technology Project (2022ZD0208100 to ZL), Shenzhen Science and Technology Program (JCYJ20220818102810022, JH), Basic Research Project of Shenzhen Natural Science Foundation (JCYJ20230807111402005 to ZL), The Key R&D Plan of Shaanxi Provincial Department of Science and Technology (2023-YBNY-184 to ZL).

Data availability

All data generated or analyzed during this study are included in this published article and its Additional file 4. Raw data that support the findings of this study

are available from the corresponding author, upon reasonable request. The accession number for the entire 16 S rRNA sequencing dataset reported in this manuscript is NCBI BioProject: PRJNA1100227 https://www.ncbi.nlm.nih.gov/bioproject/.

Declarations

Ethics approval and consent to participate

Human samples were not used in this study. All animal procedures were performed in accordance with the local welfare legislation and approved by the Animal Ethics Committee of Northwest A&F University (No. XN2023-0716).

Consent for publication

Not applicable.

Competing interests

The authors declare no competing interests.

Author details

[1]College of Food Science and Engineering, Northwest A&F University, Yangling 712100, Shaanxi, China
[2]Department of Neurology, Peking University Shenzhen Hospital, Shenzhen 518000, Guangdong, China
[3]Northwest A&F University Shenzhen Research Institute, Shenzhen 518000, Guangdong, China

Received: 27 May 2024 / Accepted: 5 August 2024
Published online: 12 August 2024

References

1. Si ZZ, Zou CJ, Mei X, Li XF, Luo H, Shen Y, Hu J, Li XX, Wu L, Liu Y. Targeting neuroinflammation in Alzheimer's disease: from mechanisms to clinical applications. Neural Regen Res. 2023;18:708–15.
2. Griffiths J, Grant SGN. Synapse pathology in Alzheimer's disease. Semin Cell Dev Biol. 2023;139:13–23.
3. Farrer LA, Cupples LA, Haines JL, Hyman B, Kukull WA, Mayeux R, Myers RH, Pericak-Vance MA, Risch N, van Duijn CM. Effects of age, sex, and ethnicity on the association between apolipoprotein E genotype and Alzheimer disease. A meta-analysis. APOE and Alzheimer Disease Meta Analysis Consortium. JAMA. 1997;278:1349–56.
4. 2016 Alzheimer's disease facts and figures. Alzheimers Dement 2016, 12:459–509.
5. Uddin MS, Rahman MM, Jakaria M, Rahman MS, Hossain MS, Islam A, Ahmed M, Mathew B, Omar UM, Barreto GE, Ashraf GM. Estrogen Signaling in Alzheimer's Disease: Molecular insights and therapeutic targets for Alzheimer's dementia. Mol Neurobiol. 2020;57:2654–70.
6. Xu H, Gouras GK, Greenfield JP, Vincent B, Naslund J, Mazzarelli L, Fried G, Jovanovic JN, Seeger M, Relkin NR, et al. Estrogen reduces neuronal generation of Alzheimer beta-amyloid peptides. Nat Med. 1998;4:447–51.
7. Correia SC, Santos RX, Cardoso S, Carvalho C, Santos MS, Oliveira CR, Moreira PI. Effects of estrogen in the brain: is it a neuroprotective agent in Alzheimer's disease? Curr Aging Sci. 2010;3:113–26.
8. Pompili A, Arnone B, Gasbarri A. Estrogens and memory in physiological and neuropathological conditions. Psychoneuroendocrinology. 2012;37:1379–96.
9. Lee JH, Jiang Y, Han DH, Shin SK, Choi WH, Lee MJ. Targeting estrogen receptors for the treatment of Alzheimer's disease. Mol Neurobiol. 2014;49:39–49.
10. Zhang QG, Wang R, Khan M, Mahesh V, Brann DW. Role of Dickkopf-1, an antagonist of the Wnt/beta-catenin signaling pathway, in estrogen-induced neuroprotection and attenuation of tau phosphorylation. J Neurosci. 2008;28:8430–41.
11. Goodenough S, Schleusner D, Pietrzik C, Skutella T, Behl C. Glycogen synthase kinase 3beta links neuroprotection by 17beta-estradiol to key Alzheimer processes. Neuroscience. 2005;132:581–9.
12. Russell JK, Jones CK, Newhouse PA. The role of Estrogen in Brain and Cognitive Aging. Neurotherapeutics. 2019;16:649–65.
13. Song YJ, Li SR, Li XW, Chen X, Wei ZX, Liu QS, Cheng Y. The Effect of Estrogen Replacement Therapy on Alzheimer's Disease and Parkinson's Disease in Postmenopausal women: a Meta-analysis. Front Neurosci. 2020;14:157.
14. Moreira AC, Silva AM, Santos MS, Sardão VA. Phytoestrogens as alternative hormone replacement therapy in menopause: what is real, what is unknown. J Steroid Biochem Mol Biol. 2014;143:61–71.
15. Domańska A, Orzechowski A, Litwiniuk A, Kalisz M, Bik W, Baranowska-Bik A. The Beneficial Role of Natural Endocrine Disruptors: Phytoestrogens in Alzheimer's Disease. Oxid Med Cell Longev 2021, 2021:3961445.
16. Fukumitsu S, Aida K, Ueno N, Ozawa S, Takahashi Y, Kobori M. Flaxseed Lignan attenuates high-fat diet-induced fat accumulation and induces adiponectin expression in mice. Br J Nutr. 2008;100:669–76.
17. Herchi W, Arráez-Román D, Trabelsi H, Bouali I, Boukhchina S, Kallel H, Segura-Carretero A, Fernández-Gutierrez A. Phenolic compounds in flaxseed: a review of their properties and analytical methods. An overview of the last decade. J Oleo Sci. 2014;63:7–14.
18. Frank J, Eliasson C, Leroy-Nivard D, Budek A, Lundh T, Vessby B, Aman P, Kamal-Eldin A. Dietary secoisolariciresinol diglucoside and its oligomers with 3-hydroxy-3-methyl glutaric acid decrease vitamin E levels in rats. Br J Nutr. 2004;92:169–76.
19. Chen G, Chen Y, Hong J, Gao J, Xu Z. Secoisolariciresinol diglucoside regulates estrogen receptor expression to ameliorate OVX-induced osteoporosis. J Orthop Surg Res. 2023;18:792.
20. Zhang Z, Wang S, Liu X, Yang Y, Zhang Y, Li B, Guo F, Liang J, Hong X, Guo R, Zhang B. Secoisolariciresinol diglucoside ameliorates Osteoarthritis via Nuclear factor-erythroid 2-related factor-2/ nuclear factor kappa B pathway: in vitro and in vivo experiments. Biomed Pharmacother. 2023;164:114964.
21. Zhang L, Lan Y, Wang Y, Yang Y, Han W, Li J, Wang Y, Liu X. Secoisolariciresinol diglucoside ameliorates high fat diet-induced colon inflammation and regulates gut microbiota in mice. Food Funct. 2022;13:3009–22.
22. Wang Z, Chen T, Yang C, Bao T, Yang X, He F, Zhang Y, Zhu L, Chen H, Rong S, Yang S. Secoisolariciresinol diglucoside suppresses Dextran sulfate sodium salt-induced colitis through inhibiting NLRP1 inflammasome. Int Immunopharmacol. 2020;78:105931.
23. Yu L, Xu Q, Wang P, Luo J, Zheng Z, Zhou J, Zhang L, Sun L, Zuo D. Secoisolariciresinol diglucoside-derived metabolite, enterolactone, attenuates atopic dermatitis by suppressing Th2 immune response. Int Immunopharmacol. 2022;111:109039.
24. Livingston DBH, Sweet A, Rodrigue A, Kishore L, Loftus J, Ghali F, Mahmoodi-anfard S, Celton C, Hosseinian F, Power KA. Dietary Flaxseed and Flaxseed Oil Differentially Modulate Aspects of the Microbiota Gut-Brain Axis Following an Acute Lipopolysaccharide Challenge in Male C57Bl/6 Mice. *Nutrients* 2023, 15.
25. Rom S, Zuluaga-Ramirez V, Reichenbach NL, Erickson MA, Winfield M, Gajghate S, Christofidou-Solomidou M, Jordan-Sciutto KL, Persidsky Y. Secoisolariciresinol diglucoside is a blood-brain barrier protective and anti-inflammatory agent: implications for neuroinflammation. J Neuroinflammation. 2018;15:25.
26. Ma X, Wang R, Zhao X, Zhang C, Sun J, Li J, Zhang L, Shao T, Ruan L, Chen L, et al. Antidepressant-like effect of flaxseed secoisolariciresinol diglycoside in ovariectomized mice subjected to unpredictable chronic stress. Metab Brain Dis. 2013;28:77–84.
27. Lu M, Tan L, Zhou XG, Yang ZL, Zhu Q, Chen JN, Luo HR, Wu GS. Secoisolariciresinol Diglucoside Delays the Progression of Aging-Related Diseases and Extends the Lifespan of Caenorhabditis elegans via DAF-16 and HSF-1. *Oxid Med Cell Longev* 2020, 2020:1293935.
28. Axelson M, Sjövall J, Gustafsson BE, Setchell KD. Origin of lignans in mammals and identification of a precursor from plants. Nature. 1982;298:659–60.
29. Nesbitt PD, Lam Y, Thompson LU. Human metabolism of mammalian lignan precursors in raw and processed flaxseed. Am J Clin Nutr. 1999;69:549–55.
30. Sawane K, Nagatake T, Hosomi K, Kunisawa J. Anti-allergic property of dietary phytoestrogen secoisolariciresinol diglucoside through microbial and β-glucuronidase-mediated metabolism. J Nutr Biochem. 2023;112:109219.
31. Ren GY, Chen CY, Chen WG, Huang Y, Qin LQ, Chen LH. The treatment effects of flaxseed-derived secoisolariciresinol diglycoside and its metabolite enterolactone on benign prostatic hyperplasia involve the G protein-coupled estrogen receptor 1. Appl Physiol Nutr Metab. 2016;41:1303–10.
32. Tecalco-Cruz AC, Zepeda-Cervantes J, Ortega-Domínguez B. Estrogenic hormones receptors in Alzheimer's disease. Mol Biol Rep. 2021;48:7517–26.
33. Marraudino M, Carrillo B, Bonaldo B, Llorente R, Campioli E, Garate I, Pinos H, Garcia-Segura LM, Collado P, Grassi D. G protein-coupled estrogen receptor immunoreactivity in the rat hypothalamus is widely distributed in neurons, astrocytes, and oligodendrocytes, fluctuates during the Estrous cycle, and is sexually dimorphic. Neuroendocrinology. 2021;111:660–77.
34. Llorente R, Marraudino M, Carrillo B, Bonaldo B, Simon-Areces J, Abellanas-Pérez P, Rivero-Aguilar M, Fernandez-Garcia JM, Pinos H, Garcia-Segura LM, et

al. G protein-coupled estrogen receptor immunoreactivity fluctuates during the Estrous cycle and show sex differences in the Amygdala and dorsal Hippocampus. Front Endocrinol (Lausanne). 2020;11:537.
35. Cooke PS, Nanjappa MK, Ko C, Prins GS, Hess RA. Estrogens in male physiology. Physiol Rev. 2017;97:995–1043.
36. Prossnitz ER, Barton M. The G-protein-coupled estrogen receptor GPER in health and disease. Nat Rev Endocrinol. 2011;7:715–26.
37. Brailoiu E, Dun SL, Brailoiu GC, Mizuo K, Sklar LA, Oprea TI, Prossnitz ER, Dun NJ. Distribution and characterization of estrogen receptor G protein-coupled receptor 30 in the rat central nervous system. J Endocrinol. 2007;193:311–21.
38. Bourque M, Morissette M, Di Paolo T. Neuroprotection in parkinsonian-treated mice via estrogen receptor α activation requires G protein-coupled estrogen receptor 1. Neuropharmacology. 2015;95:343–52.
39. Kubota T, Matsumoto H, Kirino Y. Ameliorative effect of membrane-associated estrogen receptor G protein coupled receptor 30 activation on object recognition memory in mouse models of Alzheimer's disease. J Pharmacol Sci. 2016;131:219–22.
40. Notas G, Kampa M, Castanas E. G Protein-Coupled Estrogen Receptor in Immune Cells and its role in Immune-Related diseases. Front Endocrinol (Lausanne). 2020;11:579420.
41. Zhang Z, Qin P, Deng Y, Ma Z, Guo H, Guo H, Hou Y, Wang S, Zou W, Sun Y, et al. The novel estrogenic receptor GPR30 alleviates ischemic injury by inhibiting TLR4-mediated microglial inflammation. J Neuroinflammation. 2018;15:206.
42. Kumar A, Foster TC. G protein-coupled estrogen receptor: Rapid effects on hippocampal-dependent spatial memory and synaptic plasticity. Front Endocrinol (Lausanne). 2020;11:385.
43. Gabor C, Lymer J, Phan A, Choleris E. Rapid effects of the G-protein coupled oestrogen receptor (GPER) on learning and dorsal hippocampus dendritic spines in female mice. Physiol Behav. 2015;149:53–60.
44. He X, Wang Y, Wu M, Wei J, Sun X, Wang A, Hu G, Jia J. Secoisolariciresinol Diglucoside improves Ovarian Reserve in Aging mouse by inhibiting oxidative stress. Front Mol Biosci. 2021;8:806412.
45. Bowers LW, Lineberger CG, Ford NA, Rossi EL, Punjala A, Camp KK, Kimler BK, Fabian CJ, Hursting SD. The flaxseed lignan secoisolariciresinol diglucoside decreases local inflammation, suppresses NFκB signaling, and inhibits mammary tumor growth. Breast Cancer Res Treat. 2019;173:545–57.
46. Yuan LJ, Wang XW, Wang HT, Zhang M, Sun JW, Chen WF. G protein-coupled estrogen receptor is involved in the neuroprotective effect of IGF-1 against MPTP/MPP(+)-induced dopaminergic neuronal injury. J Steroid Biochem Mol Biol. 2019;192:105384.
47. Yuan LJ, Zhang M, Chen S, Chen WF. Anti-inflammatory effect of IGF-1 is mediated by IGF-1R cross talk with GPER in MPTP/MPP(+)-induced astrocyte activation. Mol Cell Endocrinol. 2021;519:111053.
48. Wang XW, Yuan LJ, Yang Y, Zhang M, Chen WF. IGF-1 inhibits MPTP/MPP(+)-induced autophagy on dopaminergic neurons through the IGF-1R/PI3K-Akt-mTOR pathway and GPER. Am J Physiol Endocrinol Metab. 2020;319:E734–43.
49. Wendeln AC, Degenhardt K, Kaurani L, Gertig M, Ulas T, Jain G, Wagner J, Häsler LM, Wild K, Skodras A, et al. Innate immune memory in the brain shapes neurological disease hallmarks. Nature. 2018;556:332–8.
50. Yang X, Guo Y, Tse TJ, Purdy SK, Mustafa R, Shen J, Alcorn J, Reaney MJT. Oral pharmacokinetics of enriched Secoisolariciresinol Diglucoside and its polymer in rats. J Nat Prod. 2021;84:1816–22.
51. Peng L, Bestard-Lorigados I, Song W. The synapse as a treatment avenue for Alzheimer's Disease. Mol Psychiatry. 2022;27:2940–9.
52. Gao L, Zhang Y, Sterling K, Song W. Brain-derived neurotrophic factor in Alzheimer's disease and its pharmaceutical potential. Transl Neurodegener. 2022;11:4.
53. Amidfar M, de Oliveira J, Kucharska E, Budni J, Kim YK. The role of CREB and BDNF in neurobiology and treatment of Alzheimer's disease. Life Sci. 2020;257:118020.
54. Leng F, Edison P. Neuroinflammation and microglial activation in Alzheimer disease: where do we go from here? Nat Rev Neurol. 2021;17:157–72.
55. Clavel T, Borrmann D, Braune A, Doré J, Blaut M. Occurrence and activity of human intestinal bacteria involved in the conversion of dietary lignans. Anaerobe. 2006;12:140–7.
56. Liu Z, Dai X, Zhang H, Shi R, Hui Y, Jin X, Zhang W, Wang L, Wang Q, Wang D, et al. Gut microbiota mediates intermittent-fasting alleviation of diabetes-induced cognitive impairment. Nat Commun. 2020;11:855.
57. Plaha NS, Awasthi S, Sharma A, Kaushik N. Distribution, biosynthesis and therapeutic potential of lignans. 3 Biotech. 2022;12:255.
58. Franco OH, Burger H, Lebrun CE, Peeters PH, Lamberts SW, Grobbee DE, Van Der Schouw YT. Higher dietary intake of lignans is associated with better cognitive performance in postmenopausal women. J Nutr. 2005;135:1190–5.
59. Kreijkamp-Kaspers S, Kok L, Grobbee DE, de Haan EH, Aleman A, van der Schouw YT. Dietary phytoestrogen intake and cognitive function in older women. J Gerontol Biol Sci Med Sci. 2007;62:556–62.
60. Di Y, Jones J, Mansell K, Whiting S, Fowler S, Thorpe L, Billinsky J, Viveky N, Cheng PC, Almousa A, et al. Influence of Flaxseed Lignan supplementation to older adults on biochemical and functional outcome measures of inflammation. J Am Coll Nutr. 2017;36:646–53.
61. Greendale GA, Huang MH, Leung K, Crawford SL, Gold EB, Wight R, Waetjen E, Karlamangla AS. Dietary phytoestrogen intakes and cognitive function during the menopausal transition: results from the study of women's Health across the Nation Phytoestrogen Study. Menopause. 2012;19:894–903.
62. Setchell KD, Lawson AM, Mitchell FL, Adlercreutz H, Kirk DN, Axelson M. Lignans in man and in animal species. Nature. 1980;287:740–2.
63. Liu Q, Xie T, Xi Y, Li L, Mo F, Liu X, Liu Z, Gao JM, Yuan T. Sesamol attenuates amyloid peptide Accumulation and Cognitive deficits in APP/PS1 mice: the mediating role of the gut-brain Axis. J Agric Food Chem. 2021;69:12717–29.
64. Filardo EJ, Quinn JA, Bland KI, Frackelton AR Jr. Estrogen-induced activation of Erk-1 and Erk-2 requires the G protein-coupled receptor homolog, GPR30, and occurs via trans-activation of the epidermal growth factor receptor through release of HB-EGF. Mol Endocrinol. 2000;14:1649–60.
65. Hammond R, Nelson D, Gibbs RB. GPR30 co-localizes with cholinergic neurons in the basal forebrain and enhances potassium-stimulated acetylcholine release in the hippocampus. Psychoneuroendocrinology. 2011;36:182–92.
66. Zheng Y, Wu M, Gao T, Meng L, Ding X, Meng Y, Jiao Y, Luo P, He Z, Sun T et al. GPER-Deficient Rats Exhibit Lower Serum Corticosterone Level and Increased Anxiety-Like Behavior. *Neural Plast* 2020, 2020:8866187.
67. Xue Y, Zhang Y, Wu Y, Zhao T. Activation of GPER-1 attenuates traumatic Brain Injury-Induced neurological impairments in mice. Mol Neurobiol 2024.
68. Guan J, Yang B, Fan Y, Zhang J. GPER Agonist G1 attenuates Neuroinflammation and Dopaminergic Neurodegeneration in Parkinson Disease. Neuroimmunomodulation. 2017;24:60–6.
69. Pan MX, Li J, Ma C, Fu K, Li ZQ, Wang ZF. Sex-dependent effects of GPER activation on neuroinflammation in a rat model of traumatic brain injury. Brain Behav Immun. 2020;88:421–31.
70. Correa J, Ronchetti S, Labombarda F, De Nicola AF, Pietranera L. Activation of the G Protein-Coupled Estrogen Receptor (GPER) increases neurogenesis and ameliorates neuroinflammation in the Hippocampus of male spontaneously hypertensive rats. Cell Mol Neurobiol. 2020;40:711–23.
71. Kumar A, Bean LA, Rani A, Jackson T, Foster TC. Contribution of estrogen receptor subtypes, ERα, ERβ, and GPER1 in rapid estradiol-mediated enhancement of hippocampal synaptic transmission in mice. Hippocampus. 2015;25:1556–66.
72. Lebesgue D, Traub M, De Butte-Smith M, Chen C, Zukin RS, Kelly MJ, Etgen AM. Acute administration of non-classical estrogen receptor agonists attenuates ischemia-induced hippocampal neuron loss in middle-aged female rats. PLoS ONE. 2010;5:e8642.

Publisher's Note